ABSTRACT

SLAJUS, LILLIAN. A Late Holocene Earthquake and Paleoclimate Record from Ozette Lake, Washington. (Under the direction of Dr. Elana L. Leithold).

Megathrust earthquakes present multiple hazards to the Pacific Northwest including tsunamis, ground shaking, seiche waves, landslides, and liquefaction. To better assess the risk from seismic hazards in the Pacific Northwest and prepare for future events scientists must reconstruct past earthquakes. Ozette Lake is in Washington State and records Holocene Cascadia Subduction Zone (CSZ) earthquakes. Sediment cores from Ozette Lake have background sediment consisting of regularly space units of alternating dark colored, less dense and light colored, denser laminae. Four event layers of varying thickness interrupt the background sediment, recording past CSZ earthquakes. Event layers 1-4 are characterized by grain-size that is coarser than the laminated background sediments, generally fining upwards trends, and thickening toward the center of the lake basins. The units of alternating light and dark background laminae have dominant periodicities of approximately 15 to 75 years which correspond to Pacific Decadal Oscillation (PDO) phases. Negative correlation between PDO indices and an event-free computerized tomography scan of a sediment core provide a basis for using the PDO as a novel sediment dating technique. Through the characterization of event layer sediments, radiocarbon dating, and two PDO-based dating methods, the four event layers in Ozette Lake are determined to record turbidites resulting from Cascadia Subduction Zone ruptures Y, T2, W, and U. Ozette Lake sediments have a record of both Holocene seismicity and climate which provides additional evidence for the Cascadia Subduction Zone paleoseismic archive, enables the use of climate signals as a method of dating earthquakes, and better prepares the Olympic Peninsula for future Cascadia Subduction Zone ruptures.

A Late Holocene Earthquake and Paleoclimate Record from Ozette Lake, Washington

by
Lillian Slajus

A thesis submitted to the Graduate Faculty of
North Carolina State University
in partial fulfillment of the
requirements for the degree of
Master of Science

Marine, Earth & Atmospheric Sciences

Raleigh, North Carolina
2020

APPROVED BY:

_____	_____
Dr. Elana L. Leithold Committee Chair	Dr. Karl W. Wegmann
_____	
Dr. DelWayne Bohnenstiehl	

DEDICATION

To my incredible family for all their support and love as I pursued this adventure. Thank you for answering all my phone calls and keeping me on track when I was doubting myself. To my incredible teachers and instructors who have taught me so much about my field and life. To my friends who commiserated and complained with me at the worst of times, supported me when I needed help, and celebrated with me during our victories. To the STARR scholarship donors who funded my undergraduate degree and started my journey towards this moment.

BIOGRAPHY

I grew up in Iron Mountain, Michigan as the third of four amazing children. I spent my childhood outside on the shore of Lake Antoine and reading long past my bedtime. The landscape of the home inspired my love of geology and my fierce devotion to the Upper Peninsula. I took my talents downstate to Michigan State University for my undergraduate degree and spent my four years in East Lansing studying Environmental Geoscience, attending basketball games, and drinking coffee at Espresso Royale. Following graduation and an insane amount of cold emails, I found myself at North Carolina State University pursing a Master's degree.

ACKNOWLEDGMENTS

I would like to thank Dr. Lonnie Leithold, who has exceeded all possible expectations of an advisor. Your guidance, knowledge, and support has been invaluable in so many ways. Thank you to Dr. Karl Wegmann for taking the time to help me explore different avenues of research and for being the muscle during the core sampling campaign. Thank you to Dr. Del Bohnenstiehl who taught me the most valuable class I have every taken and taught me how to analyze and interpret my data. I would also like to express my gratitude to everyone at LacCore for their amazing guidance and facilities, and Trevor Contreras from the Washington Department of Natural for his assistance in the field. All these people made this project a joy to be a part of and have all my gratitude.

TABLE OF CONTENTS

LIST OF TABLES

LIST OF FIGURES

1. Introduction

Earthquakes in the Pacific Northwest present multiple hazards including ground shaking, landslides, and surface ruptures. These motions can trigger secondary hazards such as liquefaction, tsunamis, flooding, and seiche waves (Keefer, 2002). To accurately perform natural hazard assessments and assess the probability of future earthquakes scientists must look to paleoseismic records. By studying past earthquakes, scientists can help inform and prepare individuals living in high-risk areas such as the Pacific Northwest.

Multiple lines of geologic and archeological evidence have shown that the northern Cascadia Subduction Zone (CSZ) has ruptured with an average recurrence interval of ~500 years (Nelson et al., 2006; Goldfinger et al., 2012; Goff et al., 2020). Marine turbidites, subsided coastal marsh soils, and coastal tsunami deposits along the Pacific Ocean coasts of British Columbia, Washington State, and Oregon have been used to document earthquakes during the Holocene (Atwater et al., 1997, 2005; Clague et al., 2000**;** McMillan and Hutchinson, 2002**;** Thrush and Ludwin, 2007; Hutchinson and Clague, 2017). Turbidites in lakes are another proxy for pre-historic earthquakes in the Pacific Northwest (Atwater et al., 2003, 2014; Leithold et al., 2017, 2019).

Lacustrine sedimentary records from North America are underutilized as archives of past earthquakes in comparison to other seismically-active regions such as Switzerland and Chile (Monecke et al., 2004; Moernaut et al., 2009, 2014, 2017; Strasser et al., 2013; Van Daele et al., 2019). Deep, glacially carved lakes in western Washington State, however, are ideally positioned to record the Holocene history of great ($M_w \geq 8$) CSZ megathrust earthquakes. Refining the timing and spatial extent of past CSZ earthquakes from sedimentary archives is somewhat complicated by the difficulties of sampling penecontemporaneous organic materials that can be

dated with radiocarbon from within remobilized sediments. Furthermore, the combination of analytical accuracy and the non-linearity of the radiocarbon time scale results, in some cases, in uncertainties on the order of several hundreds of years. The combination of lacustrine paleoseismic and paleoclimate records from the same site can help constrain the timing of both records and inform scientists on the impact of past earthquakes along the Pacific Northwest coast. As shown in this thesis, sediments in Ozette Lake, Washington appear to preserve a millennial-scale record of CSZ earthquakes and the bio-lacustrine response to the Pacific Decadal Oscillation (PDO). This study examines the past ~1200 years of sediment accumulation in Ozette Lake, including the identification of turbidites deposited as a result of the last four Cascadia Subduction Zone earthquakes. Additionally, a robust PDO paleoclimate signal is preserved in the lake sediments that is applied as a new and supplementary method to constrain the ages of these pre-historic great earthquakes.

2.1 Lake Setting

Ozette Lake is located on the northwestern corner of Washington State's Olympic Peninsula (N 48.095˚, W 124.64˚). As the third-largest natural lake in Washington, Ozette Lake has a surface area of 30.6 km^2. The lake is oligotrophic to mesotrophic, has an average depth of ~40 m (130 ft), and a maximum depth of ~98 m (320 ft). The average water surface elevation is only ~9 m above sea level, and the Ozette watershed has a mean elevation of 91 m and is relatively low in relief. The lake has two primary basins: the northern basin and main basin. The main basin is dividable into two sub-basins by an elevated north-south that includes Tivoli Island where it rises above the lake surface. Big River, Umbrella Creek, and Crooked Creek are the dominant ingress streams, while the Ozette River is the egress channel, flowing out of the lake's north end into the Pacific Ocean**.**

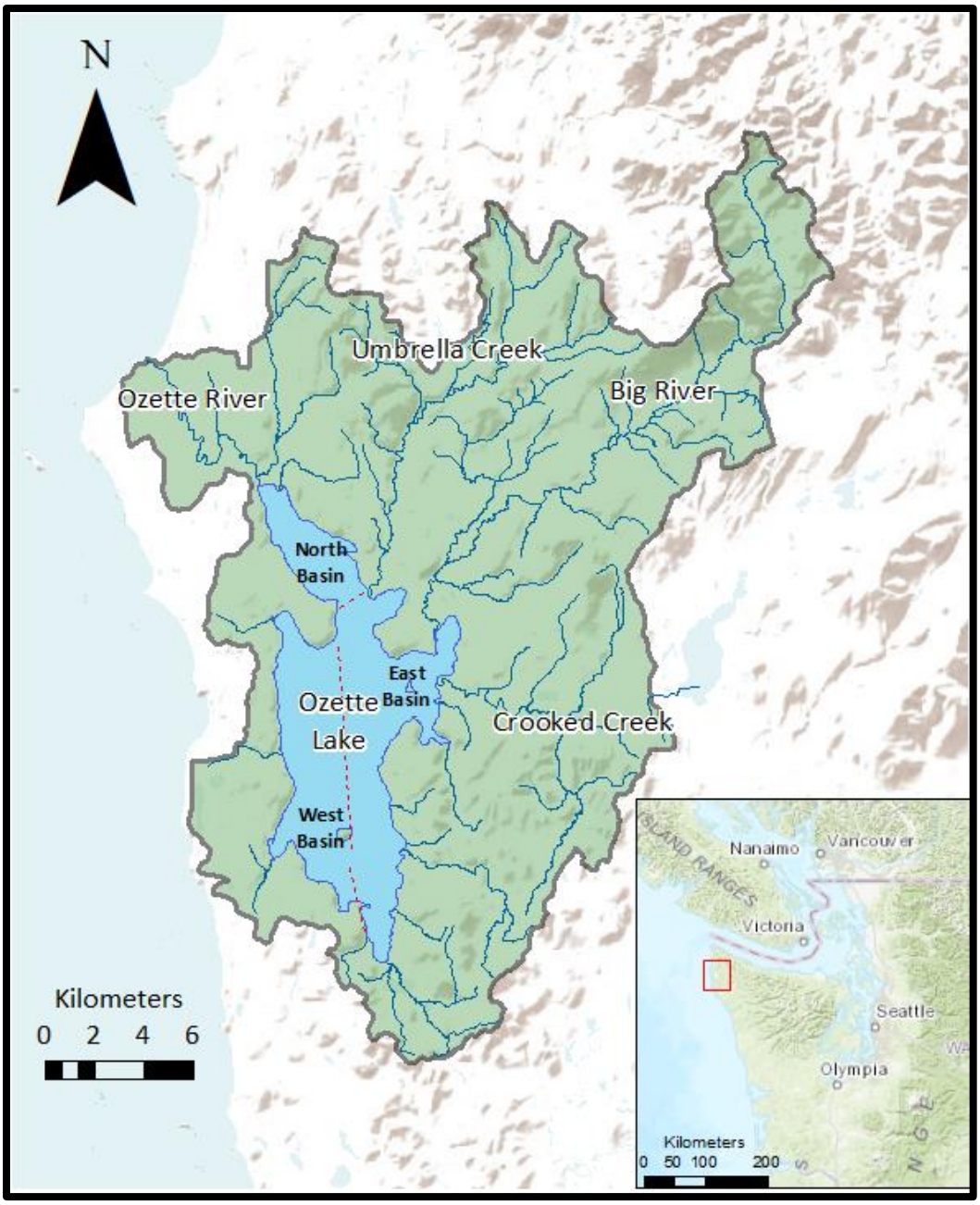

Figure 1
The Ozette watershed consists of several lakes and streams. The dominant feature of the watershed is Ozette Lake, its feeding rivers, and the Ozette River flowing out from the lake into the Pacific Ocean. Red lines divide the three subbasins.

Ancestors of the Makah, Quileute, and Klallam tribes have been managing the landscape, fishing, and living near Ozette Lake for at least ~3,600 years (McMillan, 1999; Wray and

Anderson, 2003), but due to low population numbers anthropogenic impacts on the lake were likely minimal. Commercial forestry around Ozette Lake began with European settlement in the mid-1800s and industrial forestry has continued in the area since the 1930s (Ritchie and Bourgeois, 2009). This activity has evidently resulted in increased rates of sediment accumulation in the lake, particularly after around 1960 (Ritchie and Bourgeois, 2009). Currently, Ozette Lake and the lands to the west of the lake are part of the Olympic National Park. Fifteen privately owned buildings are located on the lake shores as well as National Park Service facilities. East of Ozette Lake, the land is owned and managed by the Washington State Department of Natural Resources and several private timber companies.

1.2 Tectonic and Geologic Setting

Ozette Lake lies above the Cascadia Subduction Zone (CSZ) and is located approximately 145 km west of the Cascadia trench where the Juan de Fuca plate subducts obliquely (45˚ NE) beneath the North American Plate at a rate of ~40 mm/yr (Wells et al., 1988; DeMets and Dixon, 1999). The CSZ extends ~1,000 km from Vancouver Island to northern California. The Cascadia forearc is divided into multiple blocks that rotate in a clockwise direction due to shearing at the Pacific-North American plate boundary and westward extension of the Basin and Range province to the south (McCaffrey et al, 2007). Several small-scale Tertiary dip-slip faults to the west and north of Ozette Lake are predominantly oriented N-S along the coastline (Figure 2), whereas longer on-shore faults in the region are oriented E-W (Schasse, 2003). None of the mapped faults in the vicinity of Ozette Lake appear to offset late glacial (OIS 2) sediments, and the nearest fault with demonstrable post-glacial offset, the Sadie Creek fault is ~ 45 km to the east (Nelson et al., 2017)

Ozette Lake lies within the Cascadia accretionary wedge which is part of the Olympic subduction complex (OSC) and consists of Tertiary aged sandstone, mudstone, and basalt complexes (Brandon and Vance, 1992). The dominant formation underlying the lake basin is the Ozette Lake-Calawah Ridge block made up of Middle Oligocene - Eocene aged (25 to 55 MYA) marine sediment facies including channel fill deposits, turbidite sequences, and mélange of sandstones and basalt (Schasse, 2003). The Ozette Lake-Calawah Ridge block is exposed east of Ozette Lake and is partly covered by Late Pleistocene glacial deposits and alluvium. West of Ozette Lake the glacial outwash and till from Pleistocene glaciation covers the accreted terrane facies (Snavely et al., 1993).

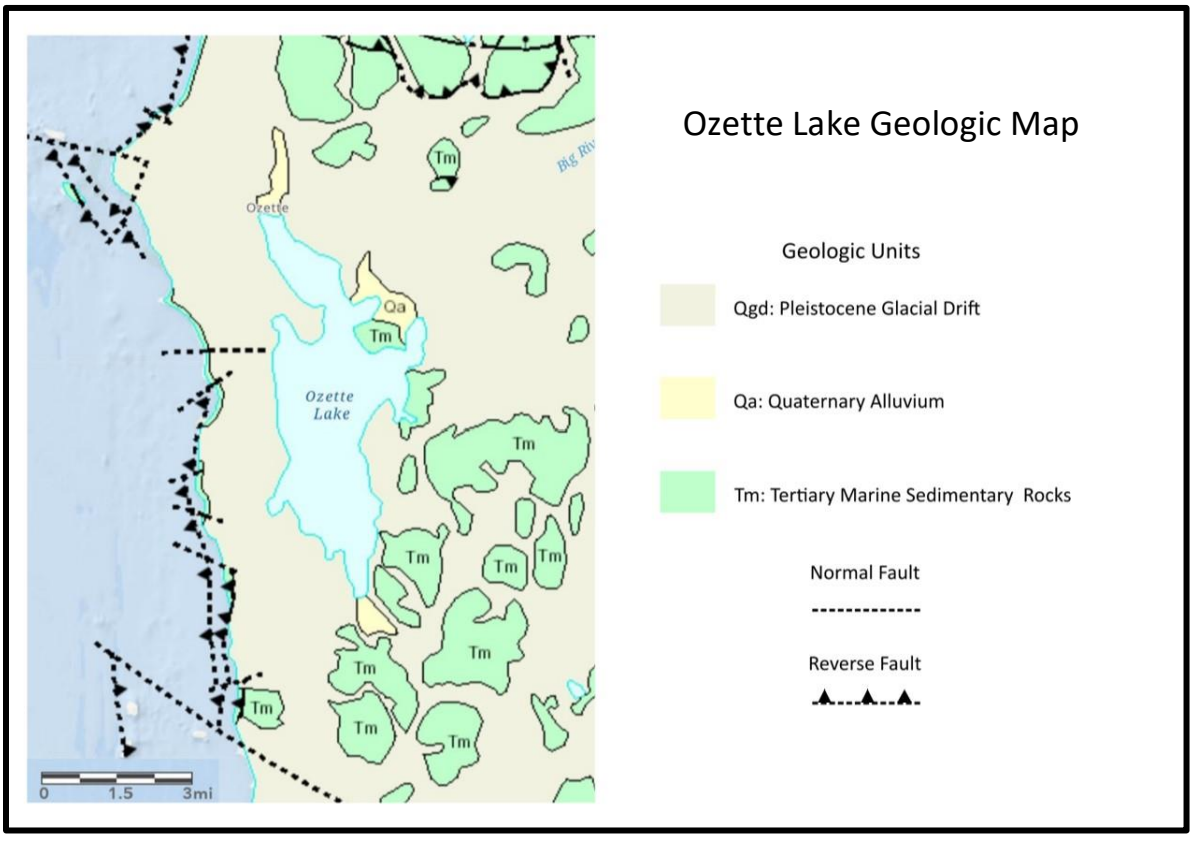

Figure 2
Simplified geologic map of the Ozette Lake basin, adapted from Schasse (2003).

1.3 Cascadia Subduction Zone Earthquakes

Due to its proximity to the CSZ and the Cascadia trench, Ozette Lake and the Olympic Peninsula are at high risk of experiencing ≥M8 megathrust earthquakes. Although there is no written documentation of earthquakes prior to 1700 CE in the region, multiple lines of evidence document repeated rupture of the CSZ throughout the Holocene. Coastal subsidence, offshore turbidites, and tsunami deposits record these megathrust earthquakes from British Columbia down to Northern California (Atwater, 1987; Goldfinger et al, 2012; Goff et al, 2020). Based on these deposits, the four most recent events have been designated, from youngest to oldest, the Y, T2, W, and U events (Atwater and Hemphill-Haley,1997; Goldfinger et al. 2003). The timing of these and earlier ruptures is debated, and the classification of megathrust earthquakes from sedimentary evidence in the Pacific Northwest is complicated by evidence of ruptures along local crustal faults (Hutchinson and Clague, 2017; Vo, 2019). Additionally, some events recorded in the northern half of the CSZ but not the southern half suggest that some of the geologic deposits record partial margin ruptures (Atwater et al., 2014; Goldfinger et al., 2012).

The four most recent megathrust earthquakes along the CSZ, which occurred during the past ca. 1400 years, have been inferred based on a variety of geologic evidence. Tsunami deposits in coastal marshes, tree rings, lacustrine turbidites, abandoned settlements, and Japanese written records were used to corroborate oral histories of the most recent great subduction earthquake, the Y event (Satake et al., 1996; Clague et al., 2000; McMillan and Hutchinson, 2002; Thrush and Ludwin, 2007; Hutchinson and Clague, 2017; Vo, 2019). Event Y occurred on January 26, 1700 as determined by written records of an orphan tsunami reaching Japan on January 27 and 28 (Atwater et al., 2005). Event T2 is identified from offshore turbidites and tsunami deposits, dated at 316-648 cal yr BP along the northern margin of the CSZ but absent

from records south of Alsea Bay, OR, which suggests that T2 may not have been a full margin rupture (Atwater et al., 2003; Nelson et al., 2006; Goldfinger et al., 2012; Hutchinson and Clague, 2017). Event W, dated to 682-914 cal yr BP, is recorded in offshore turbidites, tsunami deposits, and abandoned settlements (Hutchinson and McMillian, 1997; Goldfinger et al., 2012; Garrison-Laney, 2017; Hutchinson and Clague, 2017). Event U, dated to 1159-1327 cal yr BP, is recorded by offshore turbidites, tsunami deposits, and coastal inundation (Hutchinson and McMillian, 1997; Goldfinger et al., 2012; Garrison-Laney, 2017; Hutchinson and Clague, 2017). By comparing the lacustrine record of Ozette Lake to these previous studies, additional data can be added to the Cascadia Subduction Zone paleoseismic archive to support inferences about the timing and spatial extent of CSZ ruptures.

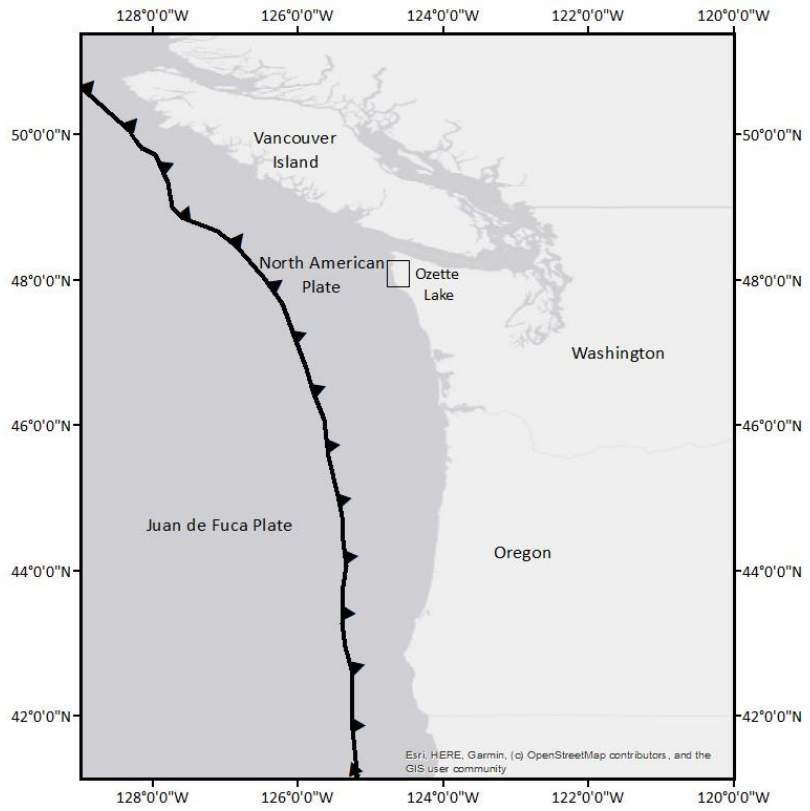

Figure 3
The Cascadia Subduction Zone extends from Vancouver Island to Northern California, approximately 1000 km. Teeth are on the overriding plate showing that the Juan de Fuca plate is subducting below the North American Plate.

1.4 Climate Cycles

Located less than 3 km inland from the coast, the lake is heavily influenced by its proximity to the Pacific Ocean with a wet season extending from September/October through April. The area experiences a wet season that is characterized by mean daily temperatures between ~4 to 10℃, ~200-250 cm of rain, and little to no snow accumulation. From the May through August "dry season", mean daily temperatures are usually 17 to 23 ℃ and the region receives ~50-75 cm of precipitation (NOAA Climate Data Record Program). In addition to seasonal climate cycles, inter-decadal ocean-atmospheric climate variability impacts Ozette Lake and the Pacific Northwest in the form of the Pacific Decadal Oscillation (PDO). The PDO is defined by North Pacific sea surface temperature (SST) anomalies driven by wind stress and sea level pressure patterns that impact precipitation, streamflow, ecosystem productivity, and land surface temperatures (Mantua et al., 1997; Hare and Mantua, 2000; Schneider and Cornuelle, 2005; Newman et al., 2016; Fang et al., 2019). Positive PDO phases are characterized by warmer SST's in the northeastern Pacific, and negative phases are characterized by cooler SST's in the northeastern Pacific, with phases lasting 20-30 and 50-70 years (Mantua et al. 1997, Zhang et al., 1997, Kaplan et al., 2000, Newman, 2016). Increased precipitation and lower surface temperatures throughout the Pacific Northwest are typical of negative PDO phases while dryer conditions with warmer surface temperatures are recorded throughout positive PDO phases (Mantua and Hare, 2002; Dong and Dai, 2015; Newman et al., 2016).

PDO indices are based on instrumental records, historical marine sea level pressure, coral SST reconstructions, wildfire records, and dendrochronology (Mantua et al., 1997; Kaplan et al., 2000; Urban et al., 2000; Biondi et al., 2001; D'arrigo et al., 2001; Gedalof and Smith, 2001; Hessl et al., 2004; McDonald and Case, 2005; D'Arrigo and Wilson, 2006; Beaufort and

Grelaud, 2017; Fang et al., 2019). The majority of reconstructed PDO indices follow a very similar pattern throughout the period of instrumental records (1900 to present) and begin to diverge for time series prior to ~1850 CE (Figure 4). Differences between time series prior to instrumental records are mainly due to the spatial variability of the proxy materials and sensitivity to local environmental conditions (Newman et al., 2016). Lacustrine sedimentary records are another proxy record for the PDO due to variations in sediment deposition that are a direct response to climate cycles (Kirby et al., 2010; Kaufman et al., 2011; Sun et al., 2013; Cerda et al., 2019). By identifying a history of relatively regularly occurring PDO cycles in lacustrine sediments, it may be possible to constrain the timing of other events, including earthquakes.

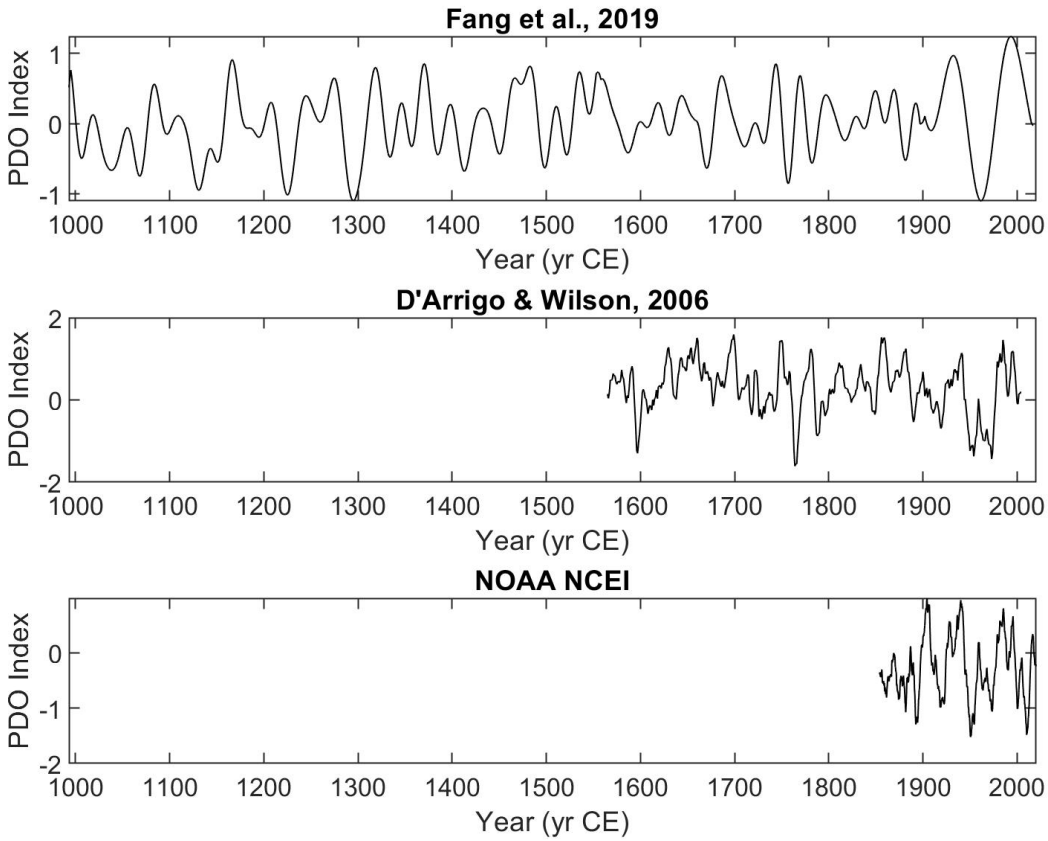

Figure 4
PDO indexes from Fang et al., 2019 and D'Ariggo and Wilson, 2006 are annual reconstructions based on synthesized tree rings records from mid-latitudes of Western North American and Asian tree ring records, respectively. The third dataset is from the National Oceanic and Atmospheric Administration's National Center for Environmental Information and was calculated from the Extended Reconstructed Sea Surface Temperature (ERSST) v5 and records the PDO on an annual scale. The five-year moving average is plotted for each data set.

2. Methods

2.1 Core Collection

In June of 2019, 18 sediment cores were collected from Ozette Lake, in partnership with the Washington Geological Survey, using a custom-built gravity corer deployed from a 5 m long motorboat (Figure 5). Fourteen sites were selected based on the bathymetry of Ozette Lake and the locations of previously collected cores by Ritchie and Bourgeois in 2005 (Ritchie and Bourgeois, 2009). Sites 2, 6, 10 and 12 were selected on the observation of visible sediment

layers in X-radiographs from sites sampled by Ritchie and Bourgeois (2009). The remaining core sites were chosen to sample from the deepest parts of the East and West sub-basins that make up the main basin of Ozette Lake. Duplicate cores were recovered at four sites (6, 7, 8, and 11).

The gravity corer consisted of a metal head weighing 4.5 kg with 22.5 kg of additional diving weights attached for a total weight of 27 kg, and a 108 cm long polycarbonate tube with a diameter of 7 cm. The polycarbonate tube was attached to the metal head and sealed with silicone lubricant and electrical tape. The gravity corer was then slowly lowered on a rope over the side of the boat. To maintain the upright position of the corer, the device was stopped at several depth increments to maintain a vertical orientation in the water column. As the device approached the lake bottom, the rope was released so the corer could fall under the influence of gravity into the sediment. To retrieve the sediment cores, the rope was attached to a mechanical crab pot puller and slowly raised up to the side of the boat. Cores were capped by hand before they were taken out of the lake. Zorbitrol, a sodium polyacrylate gel, was used to fill any space remaining at the top of the cores which were then capped and sealed with electrical tape. Coarse sediment at some site locations prevented the full 108 cm of polycarbonate tube from entering the lake sediments. In these cases, the tube was cut down to a shorter length before the addition of Zorbitrol and capping. Some cores also overflowed with sediment during capture, resulting in loss of the sediment-water interface. Once collected, the 18 cores were cut down above the sediment if needed, and packaged for ground shipment from Port Angeles, Washington to the National Lacustrine Core Facility (LacCore) in Minneapolis, Minnesota where they were stored at 4 °C.

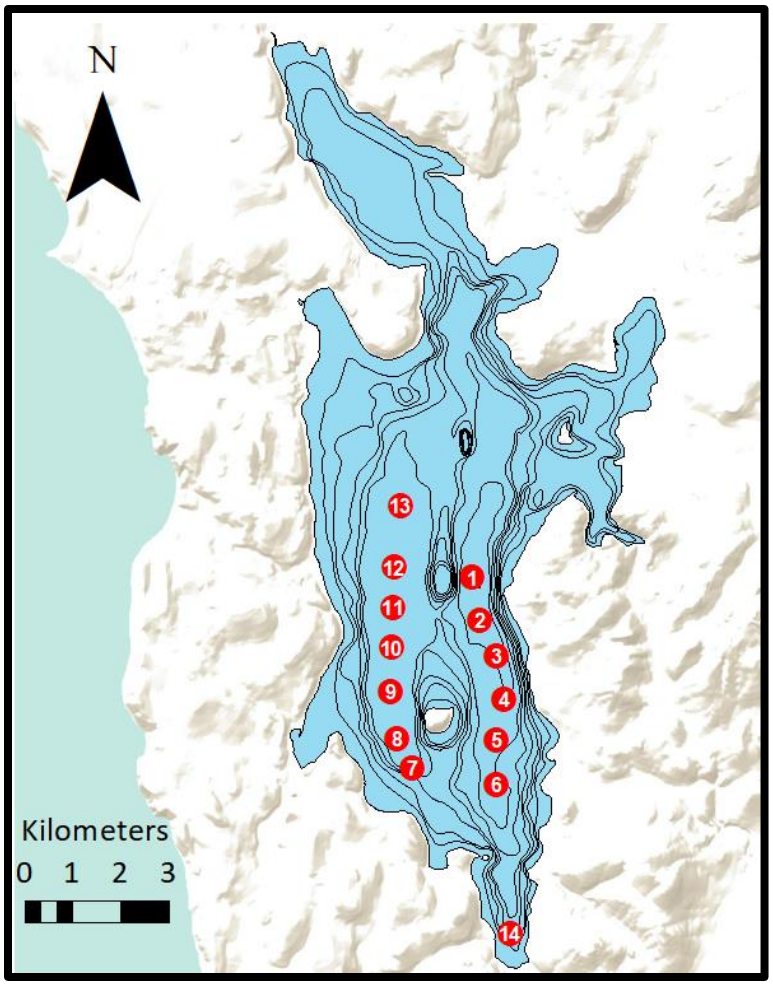

Figure 5
The 14 sampling locations (red) for this study of Ozette Lake with bathymetric contours. Cores 1-6 are were taken along a N-S track throughout the East Basin of the lake. Cores 7-13 were taken along a N-S track throughout the West Basin. Core 14 was taken at the Southernmost point of the lake. Duplicate cores were captured for sites 6, 7, 8, and 11. Due to drifting of the boat during deployment of the coring equipment, duplicate cores were taken in the vicinity of their paired core but not at the exact same position.

2.2 Core Processing

Upon arrival at LacCore, the 18 cores were scanned with a Geotek multi-sensor core logger (MSCL). Each core was measured for sediment gamma-wave density, acoustic wave velocity, electrical resistivity, and loop-sensor magnetic susceptibility at 1 cm resolution. All cores were split lengthwise using two cast saws, excluding 11B which was preserved intact for CT analysis. Any remaining polycarbonate fragments along the edges of the tube halves were

shaved off using a box cutter. The cut tubes were placed on a Schnurrenberger-Hilleshiem (Wagner modification) device where two guillotines were placed along the split edge of the tube. A box cutter was used to cut through the remaining caps, and the guillotines were pushed into the sediment cores to fully split the cores into a working half and an archival half. The faces of the split cores were smoothed and cleaned using rounded glass slides. After the cores were smoothed to a level surface, the working halves were photographed with a digital line scanner, the Geotek Geoscan-III, at 10 pixels/mm or ~300 dpi. Archival halves were scanned with the Geotek MSCL-XYZ core scanner for magnetic susceptibility and color spectrophotography data a 0.5 cm increments. Color parameters obtained include spectral reflectance at 10nm intervals for visible light between 360 nm and 730 nm, greyscale reflectance, CIE XYZ, and L*a*b* values. Archived cores were packaged for storage at the National Lacustrine Core Repository at LacCore.

Sediment and radiocarbon sampling also were conducted at LacCore. Physical sampling of the cores was conducted using steel spoons and spatulas by measuring out 0.5 cm to 1 cm thick sections that extended halfway across the split core. Samples were taken from regular intervals throughout the whole core and from layers of interest. Organic-carbon was sampled throughout the cores for radiocarbon dating. Fir needles, leaf fragments, and twigs were sampled strategically above, within, and below layers of interest. Working core-halves were packaged for storage at LacCore after the completion of sampling. All samples were frozen and shipped to the sedimentology lab at North Carolina State University.

2.3 Particle Size Analysis

Particle size was measured on samples from cores 6A and 9A. Samples from 6A were pretreated with hydrogen peroxide following the method of Gray et al. (2010) to remove the

large quantity of visible organic matter. The samples allowed to thaw for 1 hour before analysis. Once thawed ~50mg of each sample was transferred to a sterilized 50 mL beaker, submerged in 30% hydrogen peroxide, and place in a water bath maintained at ~70 ℃ with a hotplate. Samples were checked every 30 minutes to see if the hydrogen peroxide was bubbling. As the hydrogen peroxide evaporated, more was added to the beakers until the reaction stopped. The 6A samples were diluted with deionized water and analyzed for particle size. Samples from 9A did not require pretreatment because there were not large amounts of visible, organic particles. Before particle size analysis, ~50 mg of thawed sediment from core 9A were transferred to 50 mL beakers and diluted with deionized water. Diluted samples from 9A and 6A were placed on a magnetic stir plate for ~2 minutes before small volumes of sample were transferred to the Beckman Coulter LS 13-320 laser diffraction particle size analyzer with a disposable, plastic pipette. Each sample was slowly added to the analyzer until the Polarizing Intensity Differential Scattering (PIDS) obscurity reached 40%. If the PIDS reached over 45-50%, deionized water was added to the analyzer until the PIDS lowered to ~40%. Particle size distributions were measured for sediments 0.04-2000 micrometers in diameter.

2.4 Radiocarbon Sample Preparation

Eleven organic carbon samples were selected for dating based on their position above, within, or below turbidites of interest (Table 1). Samples of fir needles, leaf fragments, and roots were selected instead of more resistant wood fragments that could record a date older than the time of sediment deposition. Samples were removed from the freezer and allowed to thaw for 1 hour before being rinsed with deionized, carbon-free water in a fine mesh stainless steel sieve. After rinsing, the samples were transferred to a 50 mL sterilized, glass beaker and covered with sterilized glass lenses. Each beaker was filled with 1 N hydrochloric acid until the samples were

fully covered with the solution. The beakers were then transferred to a water bath being maintained at ~65-70 ℃ on a hotplate for 30 minutes. After the 30-minute acid bath, the hydrochloric acid was removed from each beaker using separate, sterilized syringes for each sample. Following acid removal, 1 N sodium hydroxide was added to the beakers until the sample was submerged and the samples were then returned to the water bath for 1 hour. The sodium hydroxide was removed using the allocated syringes, replaced by and fresh sodium hydroxide solution, and the samples were allowed to sit in the water bath for another 30 minutes. The process was repeated until the solution was clear, 3-12 times depending on the sample. Once the solution was clear, the 1 N hydrochloric acid was added, and the samples sat in the water bath for an additional 30 minutes. The hydrochloric acid was then removed, and samples were rinsed with deionized water every 5 minutes until the liquid tested neutral with a pH test strip. Samples were rinsed up to 8 times depending on the sample. Once neutral, the remaining liquid was removed from the beaker and the sample was placed on a hotplate to dry. All tools were rinsed with methanol, acetone, methanol, and deionized water before handling different samples. The masses of dried samples were recorded and packaged in previously sterilized glass vials. The eleven samples were sent to the National Ocean Sciences Accelerator Mass Spectrometer facility (NOSAMS) at Woods Hole Institute of Oceanography for radiocarbon analysis. Radiocarbon dates were calibrated using the Calib ^{14}C Calibration Program 7.10 and the IntCal13 curve (Reimer, et al. 2013).

The radiocarbon dates were used to determine the age of the most recent turbidite, EL 1. High-resolution core images, 10 pixels/mm or ~300 dpi, with intact water-sediment interfaces were used to locate the depth of the top of this layer in each core. The depth was then divided by age of EL 1 to determine the accumulation rate for this time interval. Radiocarbon dates were

used to construct an age-depth model using the R software program, BACON, which uses Bayesian statistics to reconstruct accumulation histories (Blaauw and Christen, 2011).

Table 1
Information for the eleven radiocarbon samples sent for C-14 analysis. Section depths were measured as a depth from the top of the tube cap, not the top of the sediments.

Sample Number	Core	Section Depth (top)	Section Depth (bottom)	Mass (mg)
1	3A	88	88.5	0.3
2	4A	48	53	1.9
3	4A	76.5	81	1.2
6	5A	40.5	41	0.2
7	6A	48	48.5	2.8
8	10A	79.5	80	0.3
9	10A	88	90	0.7
10	9A	88	88.5	0.1
11	13A	93	94	0.8
13	9A	105	107.5	4.7
15	8A	49	49.5	0.4

2.5 CT Analysis

Core 11B was preserved as a whole core and sent from LacCore to the Institut National de la Recherche Scientifique, Centre - Eau Terre Environnement in Québec City, Canada. The whole core was analyzed using a Siemens SOMATOM Definition A S+ 128 computerized tomography (CT) scanner. A composite core image with a resolution of 40 pixels/cm was made from the coronal and axial images using the SedCT: MATLAB tool kit, following the procedure of Reilly et al. (2017). Each pixel value from the composite image reflects the density measurements captured by the X-Rays from the CT scan. The composite CT image was processed using MATLAB software (MathWorks, 2019) to remove the signal from the plastic tubing, Zorbitral, and gas bubbles. Event layers (turbidites) were trimmed from the CT image to create a record of "background" sediment accumulation. Median pixel values for each row were

calculated to minimize variation through the cross section of the core. The final CT scan rendering was made by detrending these values to eliminate the effects of changes in porosity with progressive sediment loading that impact the density of sediments in the core. The image was then converted to a matrix of pixel values, and a time series was constructed using the accumulation rate calculated for the West Basin. A Fast Fourier Transform (FFT) was conducted on the time series in MATLAB to identify repeating cycles in the pixel values. Correlation coefficients were also calculated in MATLAB to compare the CT signal to the density signal from the Geotek MSCL gamma-wave density data.

2.6 Climate Signal Analysis

Three PDO indices with annual resolution were analyzed using a Fast Fourier Transform to identify repeating cycles in index values. Two PDO index reconstructions based on tree ring data were analyzed with data from the World Center for Paleoclimatology: D'Arrigo and Wilson (2006) and Fang et al. (2019). The D'Arrigo and Wilson (2006) index was reconstructed from 70 tree-ring chronologies from eastern Asia, whereas, the Fang et al. (2019) index is a synthesized record of two western North American tree-ring chronology based PDO reconstructions: Biondi et al., (2001) and MacDonald and Case (2005). The third PDO index is the National Centers for Environmental Information (NCEI) index which is based on NOAA sea surface temperature reconstructions using Extended Reconstructed Sea Surface Temperature (ERSST) v5 record. The three PDO indexes were also compared graphically to the event-free CT.

Two PDO-based dating methods independent of the radiocarbon analysis were used to determine the ages of the event layers. An average phase length of 20-30 years and 28 years (from NCEI PDO Index FFT results) for the PDO was used to date event layers within the event-free CT record by counting how many times the CT intensity crossed over the median CT

intensity value. The number of times the CT record crossed the median value was then divided by the average PDO phase length to determine a range of ages for the event layers. Wiggle-matching of the Fang et al. (2019) synthesized PDO record and the event-free CT was also used to date the event layers. Wiggle-matching aligns patterns between different proxy records to build an age-model and is an established method of dating lake sediments (Hormes et al., 2009, Snowball et al., 2010, Rey et al., 2019). The depth profile of the event-free CT, filtered using a bandpass filter in MATLAB to show periodicities between 14 and 75 years, was manually wiggle-matched to the Fang et al. (2019) PDO index by compressing and stretching segments of the PDO index to align matching patterns in the records. The filtered CT record was used to eliminate longer and shorter cycles from non-PDO environmental and climatic influences, and the compression and stretching of the PDO index accounted for changes in sediment accumulation rate with time. The ages from the PDO index that aligned with the depths of the event layers were then used to date the event layers.

3. Results

3.1 Core Description

The cores consist of light tan to brown, silty clay with millimeter-scale laminations interstratified with up to four thicker and coarser event layers. The laminated sediment is interpreted to record every day or "background" sediment accumulation in the lake. Predominantly lighter colored silt laminae in 3-5 cm-thick groupings alternate with darker groupings of laminae of the same thickness throughout the cores. Organic fragments including leaves, fir needles, roots, and wood debris are disseminated throughout the background sediment.

Event layers (EL) 1-4, interpreted as turbidites, differ from the background sediment in particle size and arrangement, thickness, and concentration of plant debris. Event layer bases

begin with an abrupt increase in grain size relative to the underlying sediments, increase in organic debris, and darkening in color. Turbidite thickness ranges from 0.5 cm to >69 cm, with internal sediments fining upwards from medium to fine sands to fine silt. Some layers are composed of multiple, stacked fining-upwards layers. A distinct, light colored clay cap, up to 1 cm thick, tops most turbidites. Turbidite thickness varies throughout the lake and between each basin (Table 2). The turbidites follow the bathymetry of the lake basins, ponding at the deepest sections of the lake, which contrasts with the relatively consistent thickness throughout the lake of the units of darker and lighter laminated silt that comprise the background (Figure 6).

Table 2
Core depths and turbidite thicknesses for all cores except for core 14A. If a specific turbidite was not identified in the core, or was thinner than 0.5 cm, then no value is recorded. Tops of turbidites are recorded as the depth from the top of collected sediment. Cores with intact sediment-water interfaces are bolded. The other cores have some sediment missing from the tops of the sediment column.

Core ID	Total Core Thickness (cm)	Depth of EL 1 Top (cm)	EL1 Thickness (cm)	Depth of EL2 Top (cm)	EL2 Thickness (cm)	Depth of EL3 Top (cm)	EL3 Thickness (cm)	Depth of EL4 Top (cm)	EL4 Thickness (cm)
1A	103	34	>69	-	-	-	-	-	-
2A	**93.5**	**30**	**4**	**51.5**	**1**	**69.5**	**4**	**85.5**	**4.5**
3A	**97**	**38**	**22.5**	**81**	**9.5**	**-**	**-**	**-**	**-**
4A	**86.5**	**34.5**	**8**	**65**	**5.5**	**-**	**-**	**-**	**-**
5A	76.5	30	4	51	5	76	3.5	-	-
6A	**93.5**	**36.5**	**25**	**77.5**	**8**	**-**	**-**	**-**	**-**
6B	**98.5**	**39.5**	**19**	**78**	**5**	**-**	**-**	**-**	**-**
7A	72	26	1	50	1	64	0.5	-	-
7B	99	26	1	47	1	61.5	0.5	82	0.5
8A	58	11	3	33	3	54	2	-	-
8B	**74**	**11**	**3**	**30**	**3.5**	**51.5**	**4.5**	**-**	**-**
9A	**95**	**28**	**3**	**49.5**	**1.5**	**70**	**2.5**	**90**	**4**
10A	99.5	29.5	10.5	-	-	83	8	106	
11A	**69**	**31**	**6**	**-**	**-**	**-**	**-**	**-**	**-**
11B	91.5	30	3	-	-	57.5	2	90.5	2
12A	**96**	**28**	**3**	**-**	**-**	**70.5**	**2**	**86**	**0.5**
13A	**93.5**	**30**	**1**	**-**	**-**	**68**	**1.5**	**82.5**	**0.5**

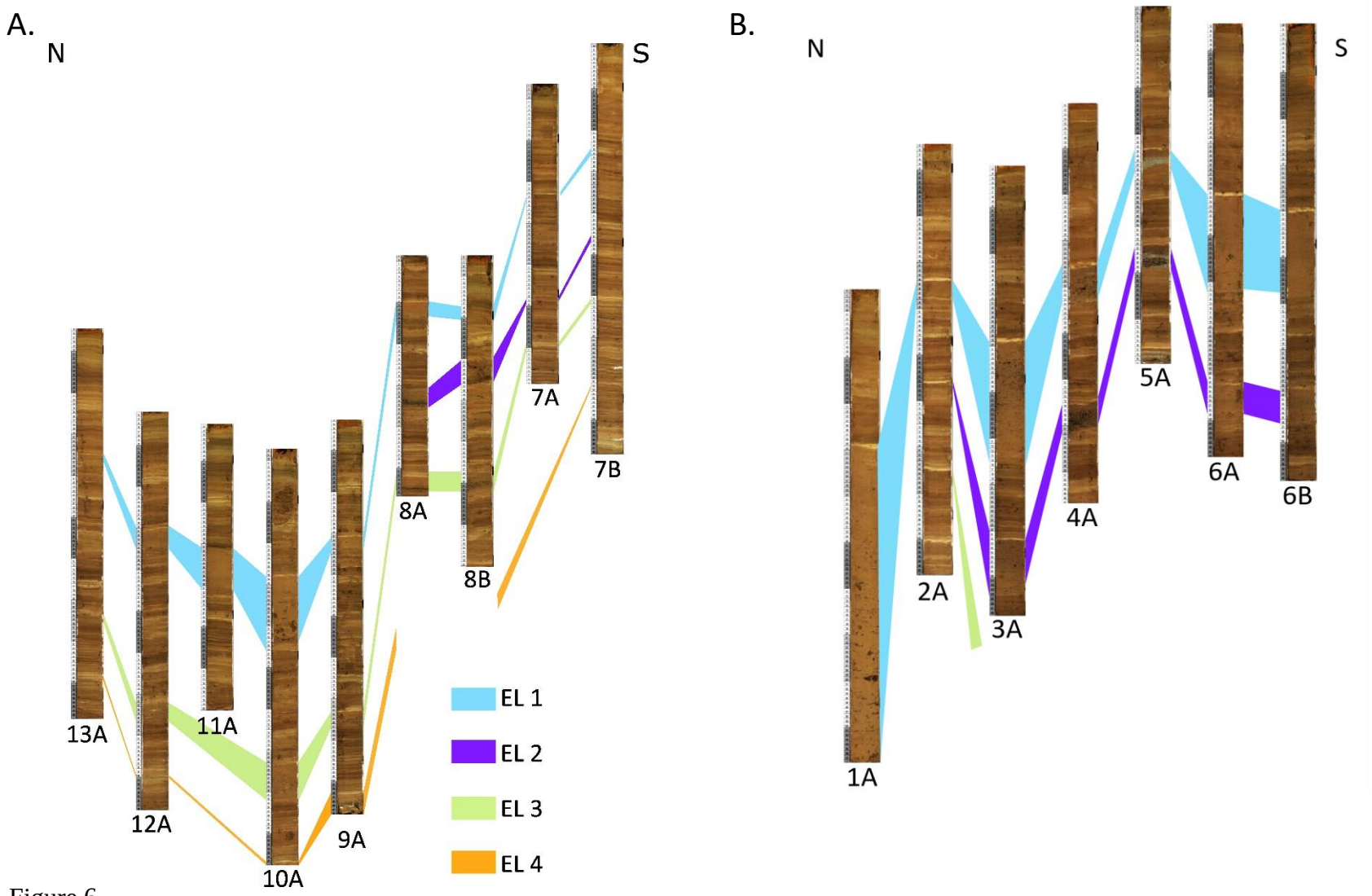

Figure 6
Distribution of the cores and the event layers throughout the West Basin, A., and the East Basin, B., of Ozette Lake. The position of the cores is proportionate to the water depth where they were recovered. All cores are shown except for 11B which was set aside for CT analysis and 14A which was from a water depth too shallow to preserve event layers.

3.2 Particle Size

Particle size analysis conducted on event layers in cores 6A and 9A exhibit similarities across cores and turbidites. The base of each turbidite in both cores was much coarser than the middle and the top of the event layers. The average percentage decrease in D90 particle size, the 90^{th} percentile of particles, from the base to the top of the turbidite was ~44% for the five turbidites analyzed in the two cores. Particle sizes ranged from 189.4 to 16.4 µm and 162.4 to 14.5 µm in diameter for cores 9A and 6A, respectively. These particle sizes fall into the fine silt to fine sand categories.

3.3 Radiocarbon Age Constraints

The eleven radiocarbon sample ages are presented in Table 3. Organic matter from within each event layer, except EL 2, are older than samples immediately below the event layers. These apparent up-core age reversals suggest that the age of sediments within the event layers is best determined from the range of ages of sediment above and below the event layer. Using this method, EL 1 was deposited between 149 to 497 cal. yr BP. The only historically documented CSZ earthquake, event Y, falls within this age range. Because event Y is known to have occurred on January 27, 1700 CE, EL 1 is assigned to this date. Core collection occurred 319 years after the event Y earthquake, and this period is used to calculate accumulation rates and as a tie point for the BACON age-depth model.

Table 3
Radiocarbon dates from fir needles and leaf fragments and their associated event free depths. All ages are calculated as years before 1950, or yr BP. Uncalibrated radiocarbon ages with 1 sigma error ranges were measured at the National Ocean Sciences Accelerator Mass Spectrometer facility (NOSAMS) at Woods Hole Institute of Oceanography. Median calibrated age and the calibrated 2 sigma age ranges were derived using the Calib ^{14}C Calibration Program 7.10 and the IntCal13 curve (Reimer, et al. 2013). Ages are grouped by position relative to the four turbidites.

Sample Number	Core	Sample Location	Event Free Depth (cm)	Radiocarbon Age BP (1 sigma)	Median Calibrated Age (cal yr BP)	Calibrated 2 sigma age (yr BP)
7	6A	above EL1	28	205+/-15	166	149-296
2	4A	within EL1	31	470+/- 15	515	504-527
6	5A	below EL1	34	310+/- 55	385	157-497
1	3A	above EL2	47	495+/-20	524	508-539
3	4A	within EL2	50	760+/-20	687	670-709
15	8A	below EL2	54	1200+/-20	1125	1064-1179
8	10A	above EL3	63	1020+/-20	940	921-963
9	10A	Within EL3	67	1210+/-25	1132	1062-1232
10	9A	below EL3	69	1010+/-210	945	559-1307
11	13A	above EL4	78	1220+/-20	1142	1067-1237
13	9A	within EL4	83	1530+/-20	1411	1355-1520

The post EL 1 median sediment accumulation rate throughout Ozette Lake is 0.096 ± 0.007 cm/yr. In the East Basin, the accumulation rate is 0.111 ± 0.005 cm/yr, while in the West Basin is 0.091 ± 0.002 cm/yr. These accumulation rates were used to as a whole core sediment accumulation rate, although sediment accumulation was likely lower down core. The average event-free depths (EFD) for each turbidite were determined by removing their thicknesses from the cores. EFDs are 31, 50, 67, and 83 cm for event layers 1 through 4, respectively. The depths for each radiocarbon sample were determined from their stratigraphic position above and below these event layers in order to run an age-depth model. Because the radiocarbon samples were

taken from multiple cores throughout Ozette Lake, the age-depth model is a composite of multiple cores and was able to represent the entire lake.

In addition to the EFDs and calibrated ages for samples above and below the turbidites and the 1700 CE calendar date for EL 1, the results from ^{210}Pb geochronology by Ritchie and Bourgeois (2009) was also used in the age-depth model. Ritchie and Bourgeois (2009) found a deflection in their ^{210}Pb profiles at about 8.4 cm beneath the water-sediment interface that signifies the year 1958 CE. The age-depth model was run without ages from within event layers and plotted the surface, the ^{210}Pb calibrated date, and the 1700 CE for EL 1 date as calendar dates using an accumulation rate of 0.1 cm/year.

Ages from within event layers were not included in the BACON model because the plant debris contained in those layers is thought to have been remobilized and is more likely to have an "in-built age" that is older than the more slowly deposited background sediments found above and below event layers. Eighty percent of the age-depth parameters input into the model fall within the 2-sigma range of the age-depth model output. Turbidite ages calibrated using the BACON age-depth relationship are compared with the radiocarbon dates in Table 4.

Table 4
Radiocarbon, calibrated, and BACON ages for the four turbidites. Each age is recorded as years before 1950, or yr BP. The BACON results are the ages calibrated for the event free depths shown in Table 3.
*age interpolated from younger layers

Event Layer	Radiocarbon Age (1-σ) (cal yr BP)	Median Cal. Age (cal yr BP)	Calibrated 2-σ Age (cal yr BP)	BACON Median Age (cal yr BP)	BACON 2-σ Age (cal yr BP)
1	470±15	515	504-527	267	227-331
2	760±20	687	670-709	604	547-707
3	1210±25	1132	1062-1232	897	828-1002
4	1530±-20	1411	1355-1520	1109*	1006-1197

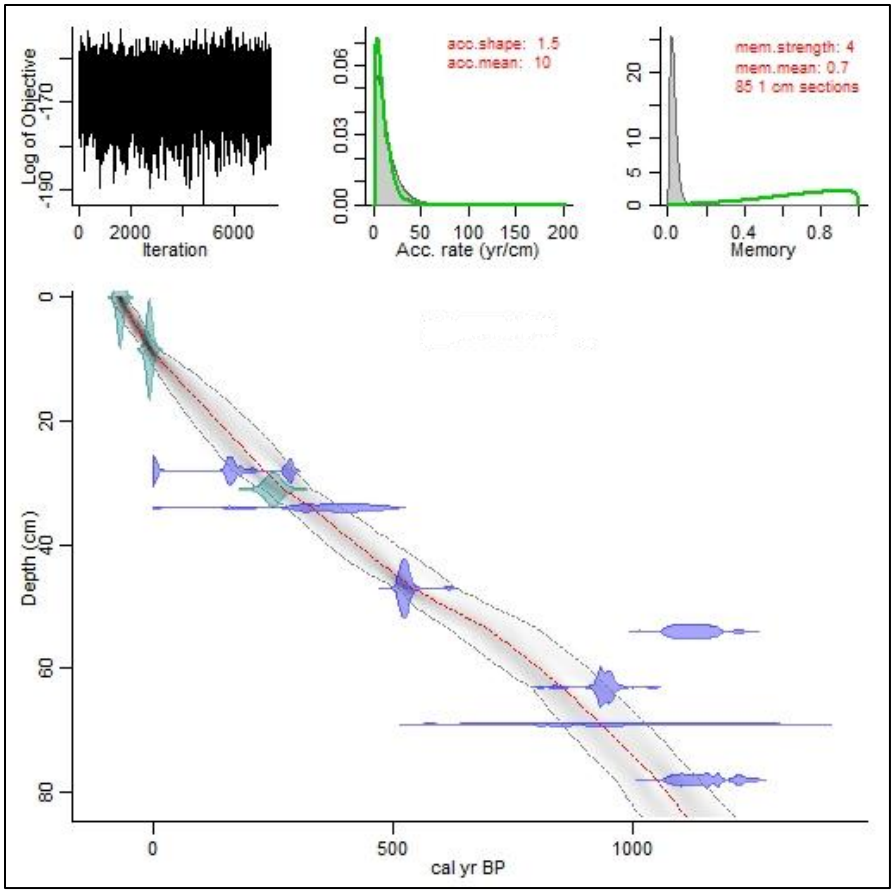

Figure 7
BACON age-depth model. Calendar dates with an error of 5 years, following BACON protocol, are plotted in teal. Zero cal yr BP is 1950 CE. Dates above and below turbidites are plotted with their respective error in purple. The grey envelope surrounding the age-depth model represents the 95% confidence envelope.

3.4 CT Analysis

The rendered and the raw CT images for both the full core and the event-free core can be seen in Figure 8. The Fast Fourier Transform results for the time series and the ten most prominent peaks in the spectral plot can be seen in Figure 9 and Table 5, respectively.

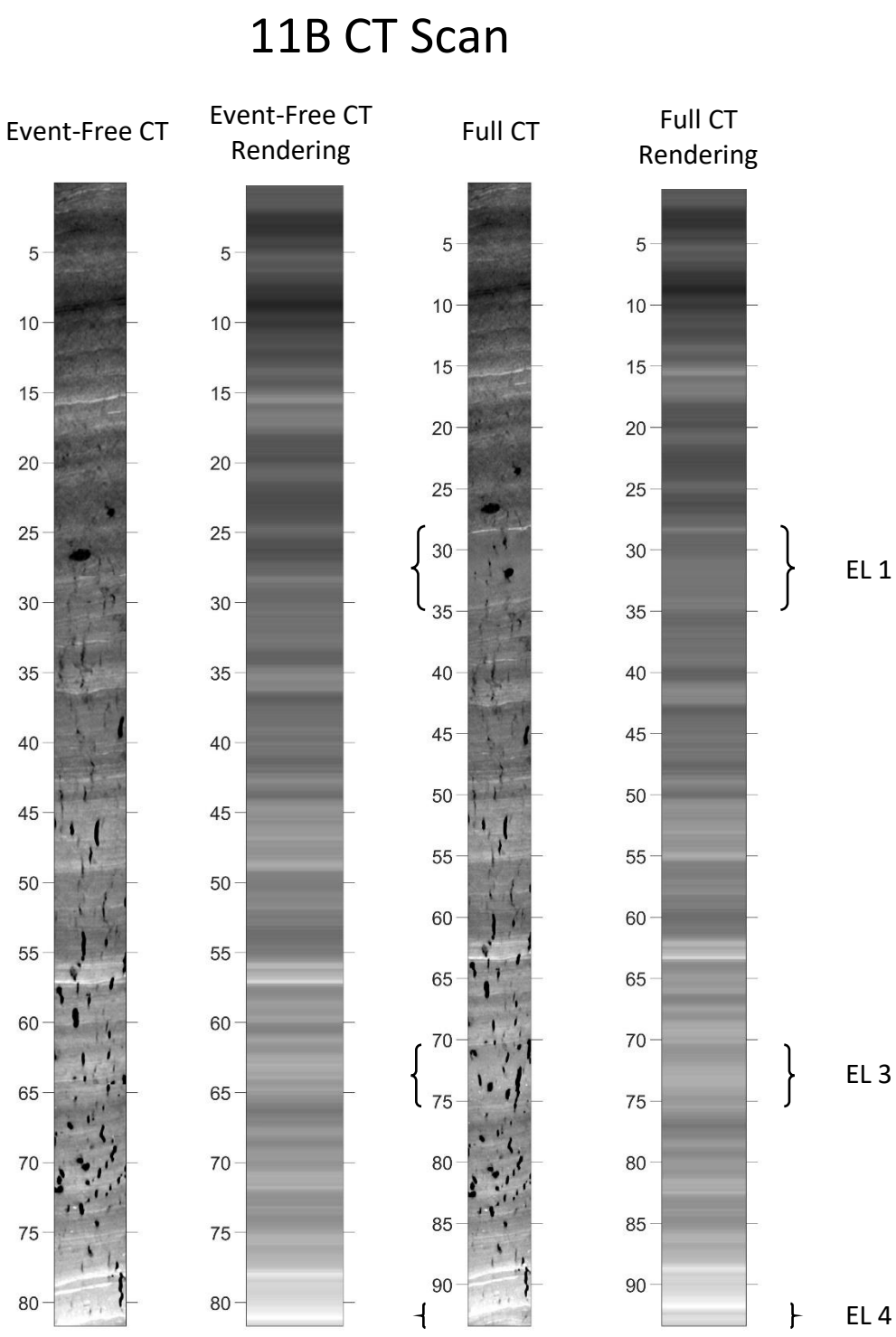

Figure 8
Images of the raw CT data and renderings are shown above for both the complete and event free records. Lighter layers have higher pixel intensities and are denser than the darker layers with lower pixel intensities. Reconstructions were made by removing bubbles and using the median pixel intensity for each row. Pixel intensities have not been detrended for these reconstructions.

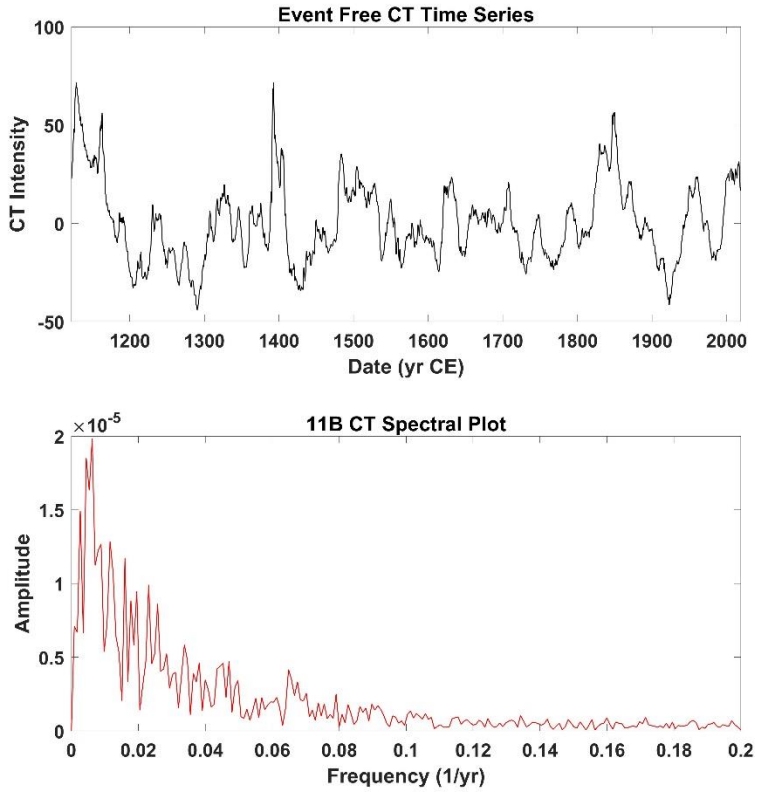

Figure 9
The event free, detrended CT time series and its FFT. The time series extends from 1162 to 2019 CE (788 to -69 yr BP) and was calculated using an accumulation rate of 0.091 cm/yr. The peak amplitude calculated with the FFT is at a frequency of 0.0062 yr^{-1}.

Table 5
Peak prominence was calculated by bootstrapping the FFT output in MATLAB, to determine the most prominent peaks in the CT intensity spectral plot. Frequencies and periods for 10 peaks are listed in the order of decreasing prominence.

Spectral Peaks										
Prominence Ranking	1	2	3	4	5	6	7	8	9	10
Frequency (yr^{-1}) x 10^2	0.62	0.89	1.78	1.33	2.31	0.27	1.96	4.44	3.47	6.58
Period (yr)	161	112	56	75	43	370	51	23	29	15

Reconstructed CT pixel intensities are proportional to Hounsfield density units but should not be used as an absolute density measurement. All CT intensities are used as a relative density measurement and signify increasing or decreasing intensity. A comparison of the detrended, 5-point moving average gamma-wave attenuation densities to the relative CT densities from pixel intensity resulted in a correlation coefficient of R= 0.5846, which supports the use of the reconstructed CT images and pixel intensities as a density measurement. Two points of divergence in the x-ray attenuation and the gamma-wave attenuation densities at depths of ~27 and ~73 cm correspond to the clay caps of event layers 1 and 3, respectively. At these depths, the CT intensity increases as gamma-wave density decreases.

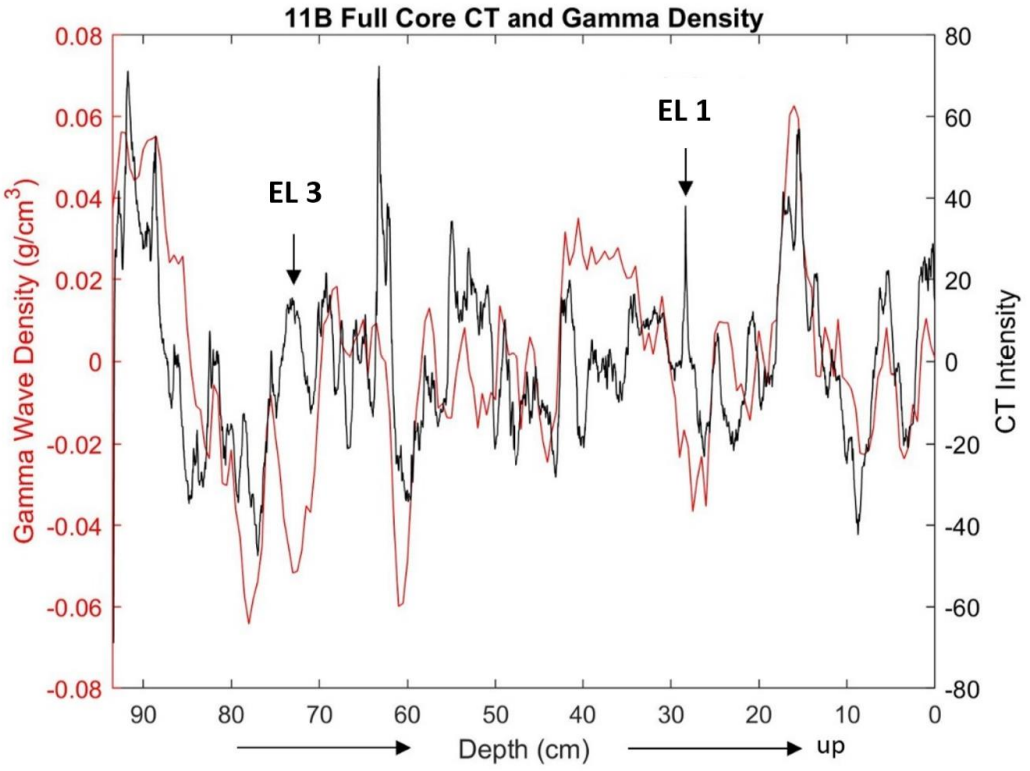

Figure 10
Detrended 5-point moving average gamma wave density, measured from gamma wave attenuation, and detrended relative CT intensity, proportional to x-ray attenuation for the full 11B core. Core depth is plotted on the x-axis. An arrow points in the up direction, towards the surface which represents the year 2019. The relative position of the top of turbidites 1 and 3 are marked with arrows.

3.5 Climate Signal Analysis

While looking for deposition cycles in the lake sediment, alternating units with relatively regular thickness comprised of lighter-colored, more dense laminae and darker, less dense laminae were observed in the cores. These cyclical units were too thick to be annual cycles, but the laminae repeat on a similar time scale as the Pacific Decadal Oscillation. The dominant periodicities for three PDO indices were calculated using a Fast Fourier Transform (Table 6). These periodicities were determined by locating the ten highest amplitudes and their corresponding frequencies from the spectral analysis. Groupings of closely spaced peaks were treated as one cycle with a range of periodicities. One result from the FFT analysis is that the longer the time series, the longer the periodicities. The NCEI PDO index, extending from 1854 to 2019 CE, has shorter cycles, 7-11 years, that are not dominant in the ten periodicities from the peak amplitudes of the Fang et al. (2019) index which extends from 993 to 2017 CE. The D'Arrigo and Wilson (2006) index extends from 1565 to 2004 CE and has peak amplitudes associated with periodicities that fall within the range of the other two indices.

Table 6
Periodicities for three PDO indexes as determined from peak amplitudes from a Fast Fourier Transform analysis. Bold values mark the periodicity of the highest amplitude for each spectral analysis. Multiple close peaks with similar frequencies are treated as one cycle with a range of phase lengths.

Pacific Decadal Oscillation Periodicities							
Fang et al. (2019)	27-32	41	53-55	62	**76**	82	93
D'Arrigo & Wilson (2006)	14-20	26-30	39	47	**57**	73	171
NCEI Index	7-11	13-19	**28**	43	85	-	-

When plotted together, the PDO indices and the reconstructed CT intensities show a negative correlation between the time series. Positive PDO indices generally align with relatively lower CT intensities from approximately 1850 to the present. Prior to ~1850 this relationship breaks down as the two PDO indices extending prior to 1850 start to disagree.

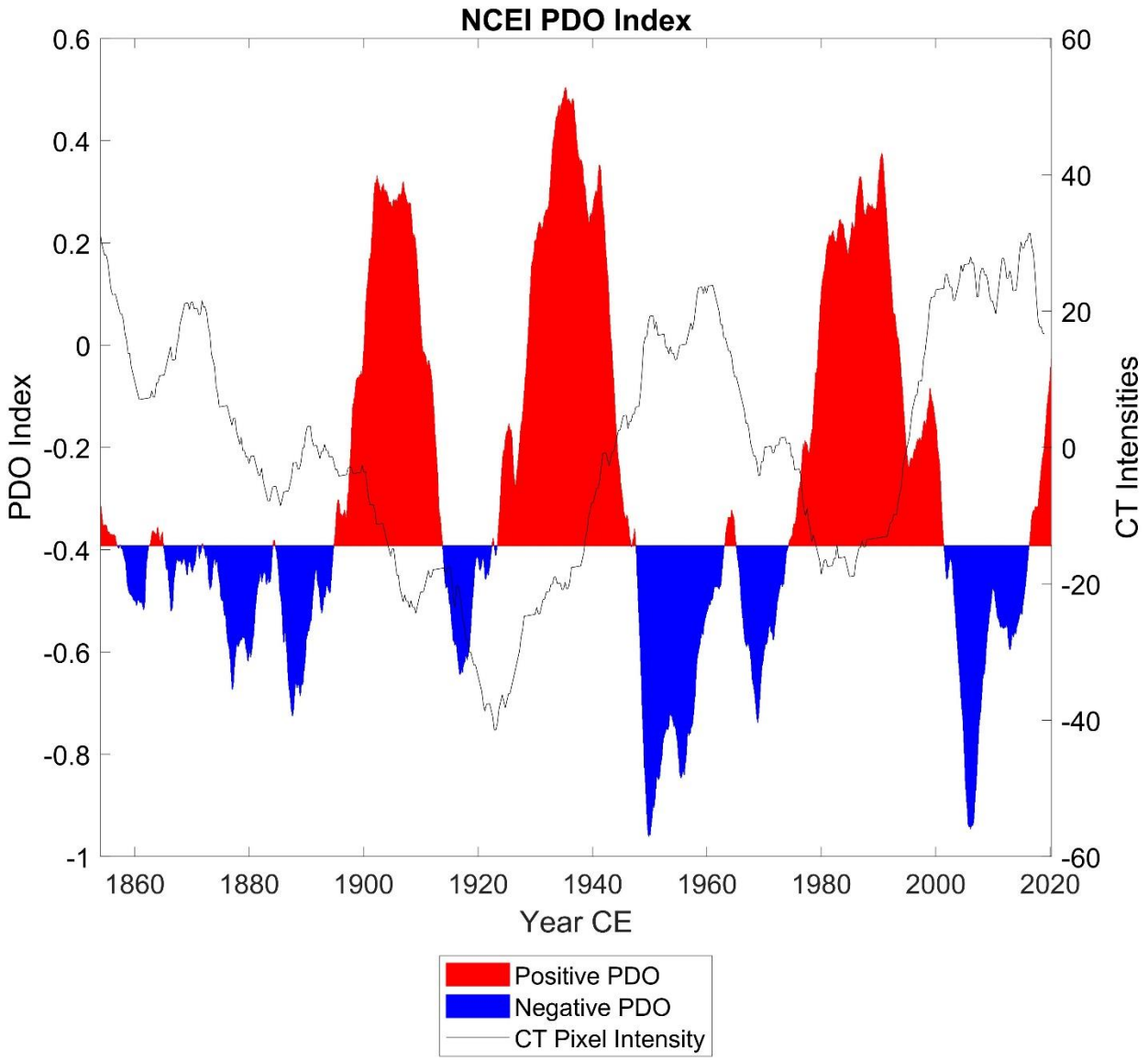

Figure 11
NCEI PDO index (five-year moving average) plotted with the rendered event-free CT intensities for core 11B. Negative PDO phases are in blue while positive PDO phases are in red.

The event-free CT was compared to the PDO indices using two different methods to further constrain the ages of the event layers. CT intensity cycles were counted using the assumption that the CT periodicities were equivalent to the shorter PDO phase length of 20-30 years. Each phase change was counted by the CT record crossing the median CT intensity value. Using this counting method, the ages of EL 1-4 range from 151-261 cal yr BP, 351-561 cal yr BP, 511-801 cal yr BP, and 791-1,221 cal yr BP, respectively. The counting method was also applied using the average phase length of 28 years, as determined from the peak amplitude periodicity of the NCEI PDO index, which results in calculated event layer ages close to the median BACON ages (Figure 12). The second method of dating the event layers using the PDO indices involved wiggle-matching the Fang et al. (2019) synthesized index to the depth profile of the event-free CT that was filtered to show periodicities between 14 and 75 years (Figure 13). The wiggle-matched ages agree with both the BACON age-depth model and the ages determined by the counting of CT cycles. An error of ±25 years (±2 cm) was used for the wiggle-matched dates to account for uncertainty in event layer depth from errors in both the trimming of event layers during the CT reconstructions and potential wiggle-match misalignment.

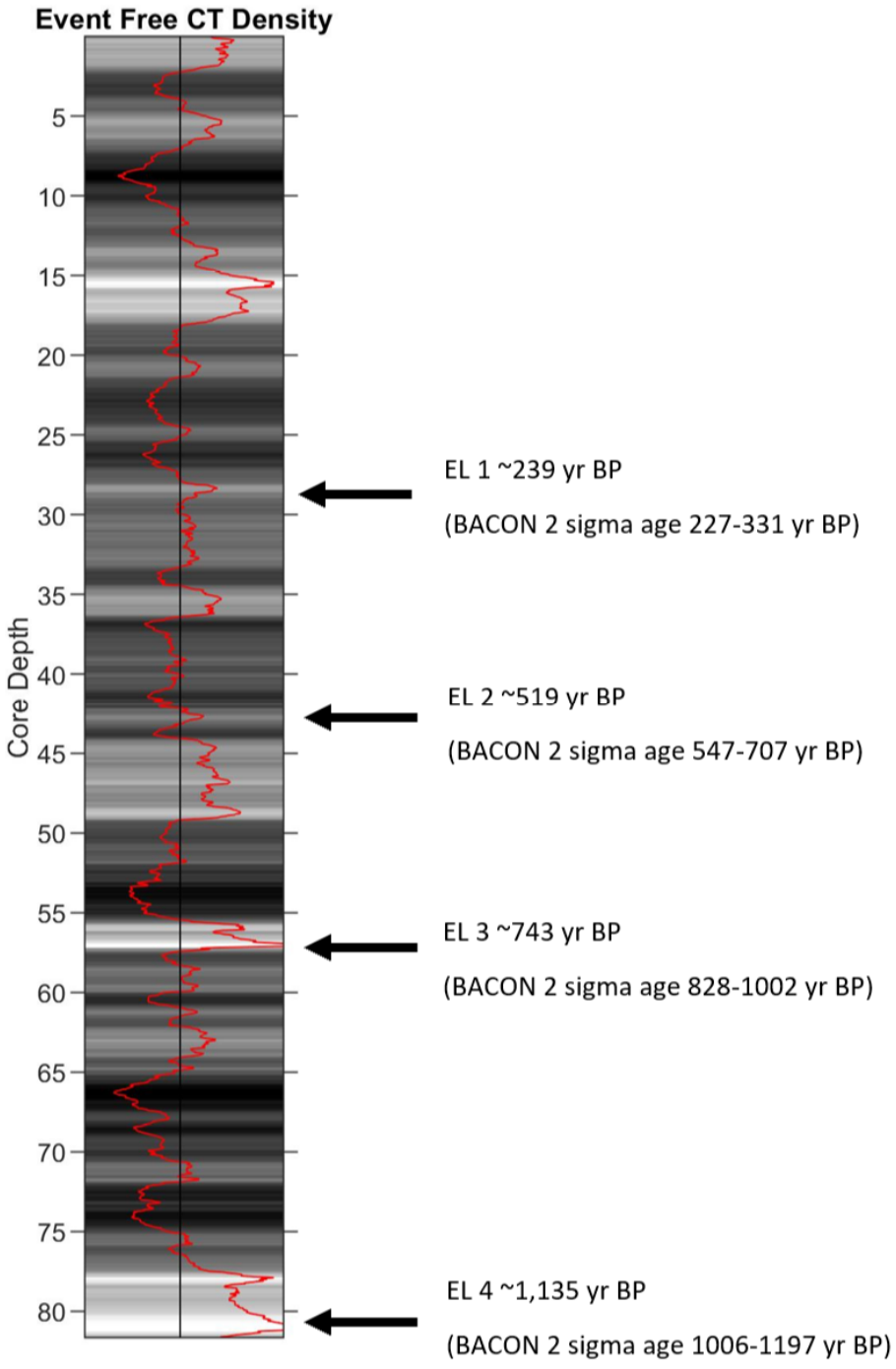

Figure 12
CT intensities are plotted over the event-free CT reconstruction. Arrows point to the depths of event layers 1-4. Ages of each event layer were calculated from the number of times the CT intensities crossed the median value (in black) using the periodicity of 28 years from the NCEI PDO index.

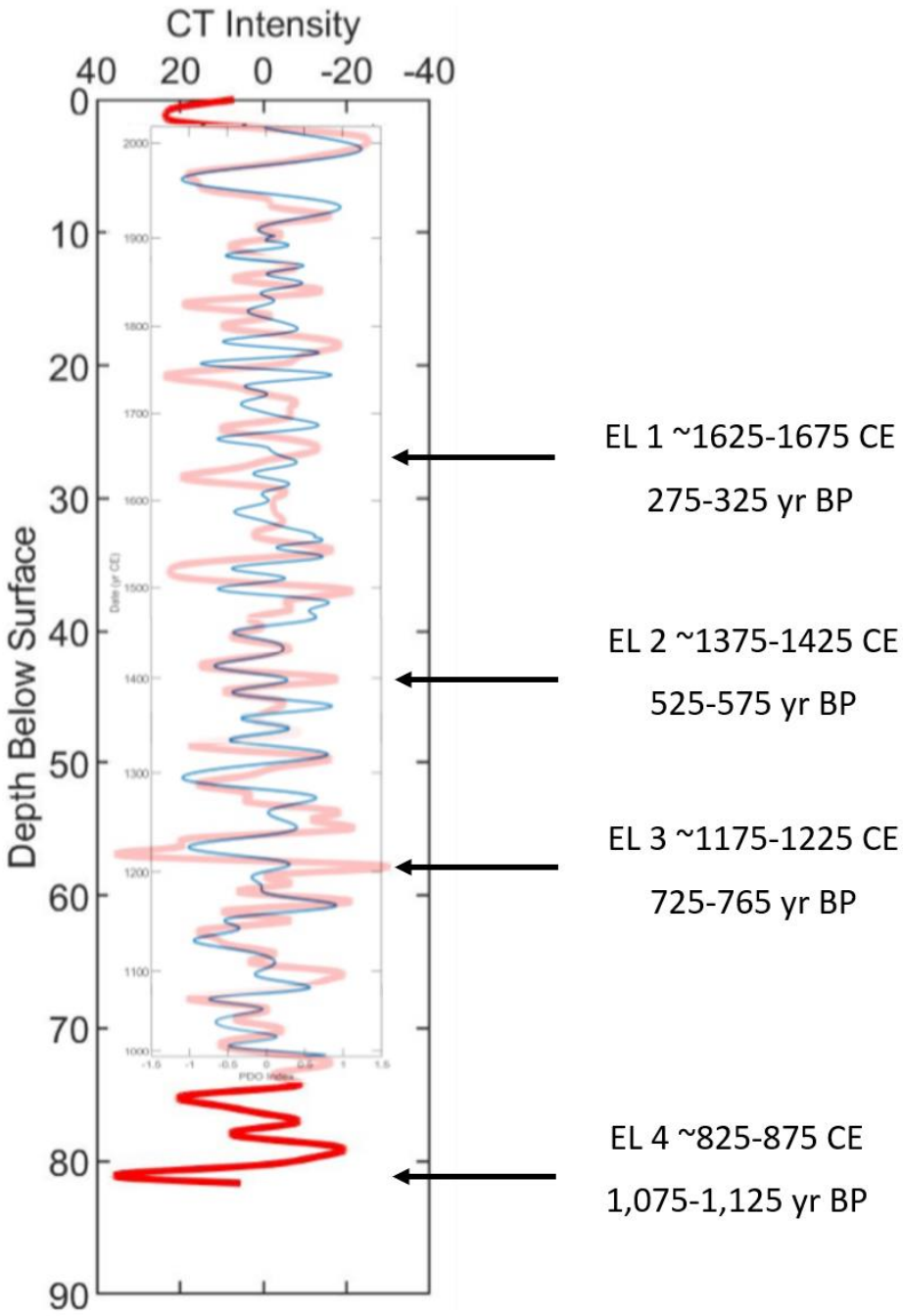

Figure 13
Event-free CT values filtered to show 14 to75 year periodicities (in red) wiggle-matched to the Fang et al. (2019) PDO index (in blue). The CT signal has been flipped across the y-axis to account for the negative correlation between the signals. Segments of the PDO index were compressed and stretched to match the patterns between the two signals. Event layer ages were determined by the PDO dates that corresponded to the depths of the event layers.

4. Discussion and Interpretation

4.1 Event Layer Interpretation

The general characteristics of the four event layers identified in the Ozette Lake cores, including grain-size that is coarser than the laminated background sediments, generally fining-upwards trends, and thickening towards the center of the lake basins, suggests that they are the product of earthquake shaking. Both river flooding and seismic activity can produce deposits that fine upwards and are thicker than the background sediments. Event layers resulting from flooding occur when in-flowing streams have high suspended sediment loads that flow into the lake basin as a hypopycnal or hyperpycnal plumes (Gilli et al., 2013). Seismically triggered event layers are deposited from turbidity currents that form when subaqueous slopes fail due to shaking (Kastens, 1984; Atwater, 1995; Goldfinger et al., 2003, 2007, 2012; Morenaut et al., 2014, 2017; Van Daele et al., 2015).

Studies of lakes with records of both recent earthquakes and flooding have provided insight into the differences in the depositional characteristics of flood and seismically induced event layers. Vanderkerkhove et al. (2020) found that the thickness of flood deposits is relatively consistent across lake basins, while seismically triggered deposits exhibit thickness variation consistent with ponding behavior. Event layer thickness at Ozette Lake follows a ponding distribution where layers are typically thicker at greater depths within the lake basin (Figure 6). Additionally, several region-wide flooding events are recorded across the Olympic Peninsula for the years of 1935, 1951, 1979, and 1995 with an estimated recurrence interval of 15 years. Stream flow measurements from USGS stations for the Sol Duc River near Fairholm, WA (Site 12041500), the Elwha River at McDonald Bridge (Site 12045500), and the Hoh River near 101 and Forks (Sites 12041000 and 12041200) all show high flow conditions corresponding to multi-

day extreme precipitation events (https://waterdata.usgs.gov/nwis/sw). There is no evidence of event layer deposition at the scale of EL 1-4 at the core depths corresponding to these dates in any Ozette Lake cores as seen in Figure 14.

Table 7
Median and peak daily discharge (ft^3/sec) for the Hoh, Elwha, and Sol Duc Rivers during January 1935, February 1951, December 1979, and November 1995 floods. The Sol Duc River does not have records after 1980.
*The Hoh River has two median daily discharges: 1,390 ft^3/sec for the station near Highway 101 which records discharge after 1960, and 1,720 ft^3/sec for the station near Forks which has records prior to 1960.

River	Median Daily Discharge (ft^3/sec)	1935 Flood Discharge (ft^3/sec)	1951 Flood Discharge (ft^3/sec)	1979 Flood Discharge (ft^3/sec)	1995 Flood Discharge (ft^3/sec)
Hoh	1,390-1,720*	22,500	19,600	39,000	30,000
Elwha	1,170	10,700	11,800	18,900	17,600
Sol Duc	351	10,800	8,300	11,800	-

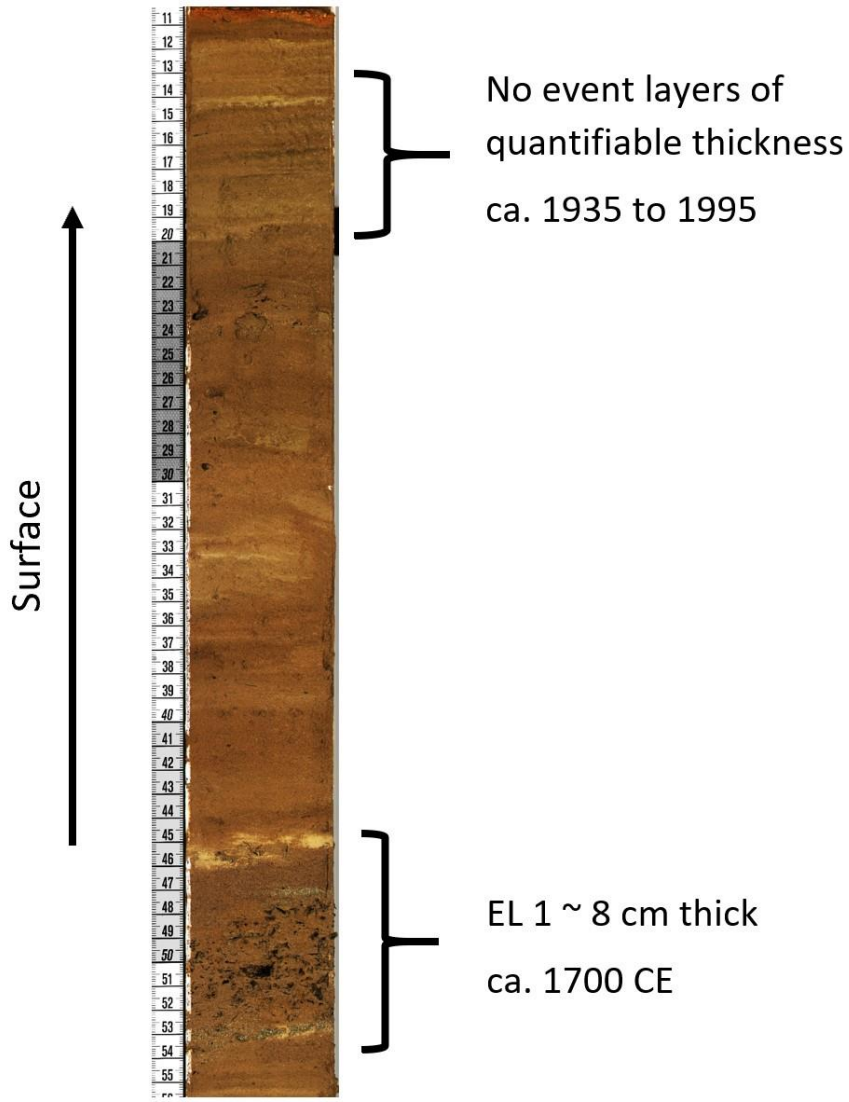

Figure 14
Core 4A comparison of EL 1 and sediment deposited from ~1935 to ~1995, during which four flooding events were recorded in the area by stream flow measurements of the Sol Duc, Elwha, and Hoh Rivers. There is no visible evidence of event layers for any of these recorded floods in Ozette Lake. Depth increments in centimeters. The water-sediment interface is preserved at 10.5 cm on the depth scale.

The presence of a fining-upwards trend from a relatively coarser base with plant debris to a clay cap, ponding of event layers at greater depth, and the lack of distinguishable deposits from recorded flooding events all suggest that event layers 1-4 were seismically triggered turbidites.

The lack of discernable event layers deposited from recorded floods does not mean that floods did not leave a signature in the cores, but do suggest that any recorded floods did not have the energy to deliver the amount of sediment mobilized through seismic shaking to the deep parts of the lake. Additionally, the lack of event layers dating to more recent earthquakes in the region suggests that the turbidites in Ozette Lake are not the result of crustal fault ruptures. Specifically, event layers dating to the 1946 Vancouver Island earthquake (M_w 7.3) or the 1872 Entiat earthquake (M_w 6.5-7.5) are not present in Ozette Lake. Together, these pieces of evidence suggest that Cascadia Subduction Zone megathrust earthquakes are the most likely seismic events to be recorded as turbidites in the Ozette Lake cores.

4.2 CT Interpretation and the Pacific Decadal Oscillation

Seasonal and annual cycles of deposition in lakes produce layers, termed varves, that are often used to reconstruct lacustrine chronologies and to supplement other dating methods such as optically stimulated luminescence, radiocarbon dating, tephrochronology, and dendrochronology (Zolitschka, 1996; Zolitschka et al., 2015). However, varves are not present in all lakes. The fine laminations in the background sediment of Ozette Lake do not appear to be regular enough to be interpreted as varves. The alternating units of lighter and darker colored laminae with relatively regular thickness in the cores appear to record decadal-scale climate cyclicity. Annual varves are formed through a combination of climate-driven variations in temperature, precipitation, biological productivity, and mineral precipitation and transport (Håkanson and Jansson, 1983). The same processes also vary over longer climate cycles such as the Pacific Decadal Oscillation (Mantua and Hare, 2002). Three indices were used to determine a relationship between the laminae in the cores and the Pacific Decadal Oscillation.

There are several shared periodicities, 26-30, 39-43, 51-57, and 73-76 years, in the Fast Fourier Transform results for the PDO indices and the CT intensities. Some of these common periodicities (28, 57, and 76 years) correspond to the peak amplitudes from the spectral analysis for each PDO index. When plotted together, the PDO and CT time series show a relatively consistent negative correlation from ~1850 to the present suggesting that for this period positive PDO phases are associated with decreased sediment density and conversely negative PDO phases are associated with increased sediment density. Multiple factors influence the density of lacustrine sediments including porosity, grain size, mineralogy, sedimentary structures, fabric, and water content (Geiger et al., 2009). Climate reconstructions from other lakes in Washington State record the influence of the PDO on precipitation and productivity which applies to Ozette Lake (Arhonditsis et al., 2004; Steinman et al., 2012).

Negative PDO phases are accompanied by increased precipitation and cooler temperatures in the Pacific Northwest. A study on the relationship between phytoplankton and the PDO in Lake Washington found higher chlorophyll and phytoplankton concentrations during negative PDO phases. In contrast, positive PDO phases have been linked to decreases in zooplankton and primary productivity along the West Coast and adjacent lakes due to increased spring and summer temperature and decreased precipitation (Hare et al., 1999; Arhonditsis et al., 2004). Winter precipitation increases associated with negative PDO phases are observed and interpreted by Steinman et al. (2012) using oxygen isotopes from Castor (Okanagan County) and Lime (Pend Oreille County) Lakes in northern Washington State. The winter precipitation reconstruction from these lakes follows the trend of the event-free CT which suggests that the CT intensities also record precipitation changes through time.

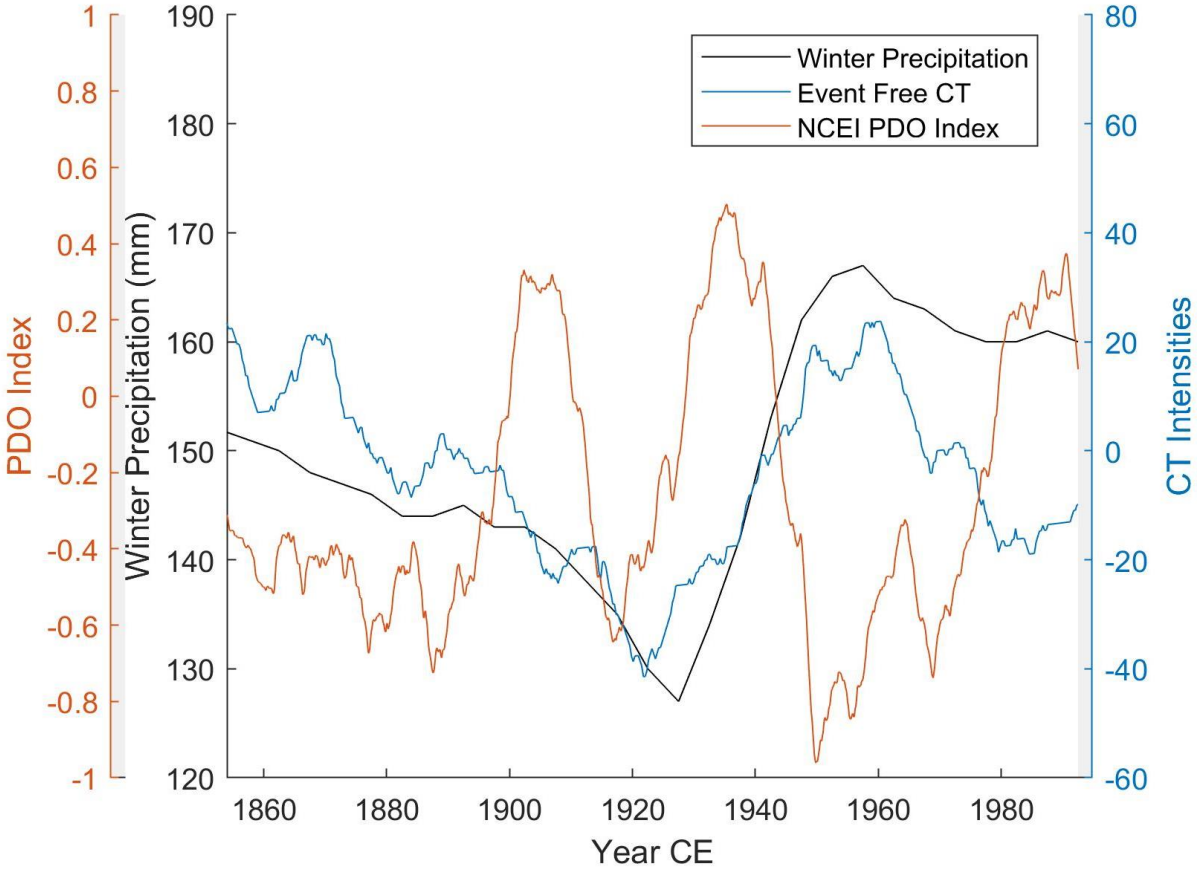

Figure 15
Winter precipitation (black) plotted with core 11B event-free CT reconstruction intensities (blue) and the NCEI PDO index (orange). The precipitation record was reconstructed from $\delta^{18}O$ values from Castor Lake and Lime Lake in Northeast Washington State.

Assuming Ozette Lake has the same precipitation response to the PDO as the other Washington lakes, the character of the lake sediments should change from one PDO phase to another. Erosion of terrestrial sediment increases as precipitation increases, leading to higher sediment loads in the streams flowing into Ozette Lake. Higher stream sediment loads increase the amount of terrestrial clay minerals entering the lake basin. Increases in sediment loads would also increase the amount of nutrients entering the lake system, causing an increase in productivity. The increased terrestrial clay input into the lake would dilute the organic fraction of lacustrine sediments. Dilution of the organic matter in the sediments makes the sediment lighter

in color and impacts the sediment density. When there is a higher concentration of clastic sediment in the water column floccules become smaller and denser (Hamm, 2002). The smaller and denser the floccules, the tighter the sediment fabric.

Conversely, during positive PDO phases when temperatures are on average higher and there is less precipitation, there is less clastic input into the lake which increases the organic fraction of lacustrine sediments. Generally, sediment with higher organic content is darker in color. A higher organic fraction of sediment increases the size of the floccules and slows their sinking velocities (Hamm, 2002). Larger, more fluffy aggregates pack together less densely than the smaller aggregates with a tighter fabric, thus helping to account for the density variation observed between the light and dark sediment units and negative and positive PDO, respectively.

Climate variability due to the Pacific Decadal Oscillation impacts sediment deposition in Ozette Lake. The core 11B density record and sediment color records these depositional changes through time which suggests that the physical properties of the sediment cores are a suitable proxy record of the PDO. When compared to other indices, Ozette Lake CT densities best match the NCEI PDO record from ~1850 to present when the reconstructions are based on aggregate sea surface temperature anomalies for the Pacific Ocean. Before to 1854, the PDO indices are based on tree rings. The PDO impacts regional climate differently based on location, and trees and lakes are under the influence of multiple environmental factors that do not relate to the PDO. Variations in climate and environment based on location and proxy method will lead to variations in different PDO reconstructions which should not be ignored, however, these inconsistencies are not enough to discount one record from another. This is especially evident when comparing the filtered CT reconstruction to the Fang et al. (2019) synthesized PDO record. Because the Fang et al. (2019) PDO index combines two PDO indices based on tree rings from

California and Western Canada, this index considers variations in PDO responses based on multiple locations which improves the ability to use this PDO reconstruction as a dating method by reducing index variations based on single locality.

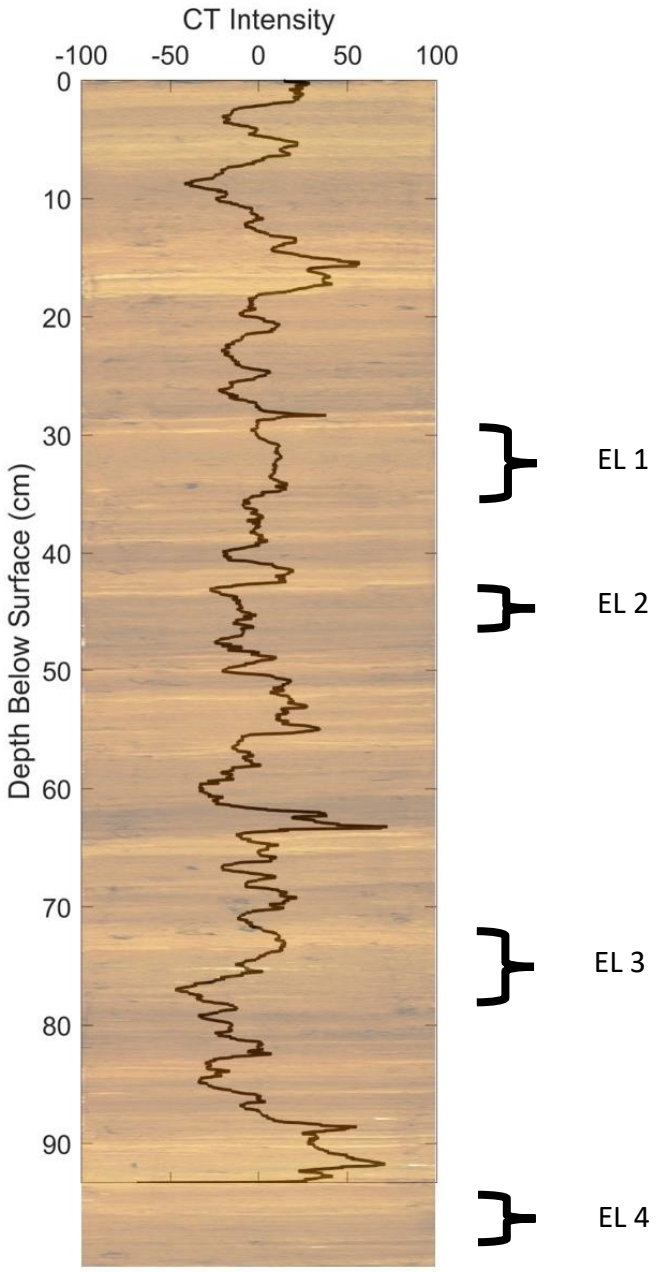

Figure 16
Reconstructed CT intensities of core 11B overlying the core image of 12A. The higher the CT intensity the denser the sediment. The approximate location of the event layers are marked with a bracket. Differences in sediment deposition at sites 11B and 12A account for misalignment of sediment color and CT intensity down core.

4.3 Dating Cascadia Subduction Zone Earthquakes

Accurately dating event layers in Ozette Lake is crucial to determining the recurrence rate of Cascadia Subduction Zone earthquakes. Not only can the ages of the turbidites help reconstruct the recurrence interval, but the location of Ozette Lake can also help to add insight into the spatial extent of shaking during specific CSZ ruptures. Although radiocarbon dating is an important tool in paleoseismic investigations, there are limitations associated with this dating technique.

Radiocarbon dating of sediment layers assumes that the organic material analyzed is the same age as the sediment in which it was derived; however, this may not always be a sound assumption. Organic material in the sediments may be much older than the surrounding sediment. Wood and conifer cones are more resilient than other plant materials and can survive transport, burial, and preservation long after plant death. The plant material used in this study was primarily fir needles and leaf fragments, which are less likely to survive transport after death, yet results indicate that at least within the turbidites themselves, these materials were significantly aged upon deposition within the event layers. Turbidites are, by definition, remobilized sediments, and it is not surprising that they incorporate previously deposited, older material from the subaqueous slopes of the lake. The intra-turbidite radiocarbon ages are interpreted as limiting maximum ages for the event layers and are not included in the BACON analysis. As such, the BACON age-depth model provides more accurate ages for the event layers than the direct dating of organic materials contained within. As an independent form of chronology, cycles of deposition attributed to the PDO were used to corroborate the BACON model.

The dates of turbidites EL1-4 were determined using a counting method. CT cycles were counted using an average PDO phase length of 20-30 years, and event layer ages calculated using this method agree with younger dates obtained with the BACON model. The PDO has two dominant periodicities, 20-30 and 50-70 years, with longer periodicities more common before the 20th century (Biondi et al., 2001; Mantua and Hare, 2002). Variations in different PDO indices makes it difficult to determine the frequency of the longer PDO phases, which is why they were not included in the PDO age model. Because the longer phases were excluded from the age model, event layers represent the youngest age ranges for the event layers or the limiting minimums. Average event layer ages calculated using the dominant phase length of 28 years, from the NCEI PDO index analysis, strongly agree with the BACON age-depth model median calibrated ages which reaffirms that this method applies to dating event layers even with the exclusion of longer PDO phases.

Additionally, wiggle-matching of the Fang et al. (2019) synthesized PDO index and the filtered CT data was used to date the event layers. Wiggle-matching does not ignore the longer phases of the PDO which means ages determined using this method are not biased towards the shorter PDO phases like the counting method. This approach also accounts for sediment accumulation rate changes throughout time. The compression of the PDO record at greater core depths accounted for decreased sediment accumulation relative to the present. Ritchie and Bourgeois (2009) document an increase in sediment accumulation after European settlement, and this trend is also captured by the BACON age-depth model. By accommodating variations in sediment accumulation rates and longer PDO phases, the wiggle-matching approach is able to provide event layer ages that strongly agree with the BACON age-depth model. Not only does this approach provide a dating method for the event layers, but it is also confirmation of a PDO

signal in the lake sediments. This observation has implications for lake ecology, including population dynamics of the Ozette Lake sockeye salmon (*Oncorhynchus nerka*), which is listed as threatened under the Endangered Species Act (National Oceanic and Atmospheric Administration, 1999, 2005, 2014; Woodward et al., 2019).

Better event layer age constraints can be obtained through the comparison these dating methods (PDO and radiocarbon-derived) because they have independent limitations and uncertainties. EL 1 has a 2-sigma age of 227-331 cal yr BP from the BACON model with an average age of 239 yr BP from the CT cycle counting method and a wiggle match age of 275-325 BP. This turbidite most likely records the 1700 CE CSZ Y earthquake event. Geologic, archeologic, and historical records document the most recent great earthquake along the full length of the CSZ, from northern California to Vancouver Island, and as far away as Japan earthquake (Satake et al., 1996; Clague et al., 2000; McMillan and Hutchinson., 2002; Thrush and Ludwin, 2007, Hutchinson and Clague, 2017; Vo, 2019). Due to the paucity of earlier written (historic) records, this is the only turbidite that can be assigned an absolute age. A phase length of 29 years resulted when a set date of 1700 CE is used to calculate the average phase length of the PDO using the counting method based on the CT record. The approach provides additional support for the use of the NCEI PDO index as an age model as a 29-year periodicity is in close agreement to the dominant 28-year period derived from the FFT analysis of the NCEI record (Table 6).

Event layer 2 has a 2-sigma BACON age of 547-707 cal yr BP with an average CT cycle count age of 519 yr BP and a wiggle match age of 525-575 yr BP. Event layer 2 is interpreted as recording the CSZ T2 rupture which Goldfinger et al. (2012) dated between 316-648 BP. The location and extent of the CSZ T2 fault rupture is debated because to date deposits of T2 age are

lacking south of central Oregon (Atwater et al., 2003; Nelson et al., 2006, Goldfinger et al., 2012; Hutchinson and Clague, 2017). The presence of T2 in Ozette Lake is not enough to determine whether the rupture was full or isolated to the northern segment of the CSZ, but it is an important addition to the CSZ paleoseismic archive.

The third event layer, EL 3, has a 2-sigma BACON age of 828-1002 cal yr BP with a CT count age of 743 yr BP and a wiggle-match age of 725-775 yr BP. These ages match up with the CSZ earthquake W which previous investigators dated to 682-914 cal. yr BP as a full-margin rupture event (Hutchinson and McMillian, 1997; Goldfinger et al., 2012; Garrison-Laney, 2017; Hutchinson and Clague, 2017). There was no plant debris in the cores below EL 4, which means that unlike EL 1-3, the BACON model EL 4 age is determined from sediment deposited more recently than EL 4. As a result, EL 4 could be older than its 2-sigma modeled age of 1006-1197 cal. yr BP. Despite the interpolated BACON age, the CT count average age of 1,135 yr BP and wiggle-match age of 1,075-1,125 yr BP suggest that the BACON model results are acceptable for EL 4. When these factors are taken into account, EL 4 is very likely the product of the CSZ U earthquake which is dated to 1010-1327 cal. yr BP by previous studies (Hutchinson and McMillian, 1997; Goldfinger et al., 2012; Garrison-Laney, 2017; Hutchinson and Clague, 2017). Using the median calibrated BACON model results with the CT cycle count and the wiggle-match ages for each event layer, the recurrence interval for the past four CSZ earthquakes is ~300±30 years. This recurrence interval is very important for the planning of future CSZ earthquakes because the last event occurred 320 years ago. Future great CSZ earthquakes off the northwest coast of Washington State are inevitable, and the likelihood increases with each passing year since January 26, 1700.

Table 8
BACON age-depth model, CT cycle count, and PDO wiggle-match ages. CSZ earthquakes, as recorded by Ozette Lake turbidites, were determined based on the ages of the event layers. Ages were determined using the BACON age-depth model, a CT cycle counting method using phase lengths of 20-30 years, and wiggle-matching of the Fang et al. (2019) synthesize PDO index and a filtered CT-depth profile.

Ozette Event Layer	CSZ Rupture	BACON 2 sigma Age (cal yr BP)	CT Counting Age Range (cal yr BP)	CT Counting Age (28 year) (cal yr BP)	Wiggle-Match Age (cal yr BP)
1	Y	227-331	151-261	239	275-325
2	T2	547-707	351-561	519	525-575
3	W	828-1002	511-801	743	725-775
4	U	1,006-1,197	791-1,221	1,135	1,075-1,125

5. Conclusions

5.1

Ozette Lake is in an ideal location in Washington State to record Cascadia Subduction Zone earthquakes. Sediment cores from Ozette Lake have background sediment consisting of regularly spaced units of alternating dark colored, less dense and light colored, more dense laminae. Four event layers of varying thickness interrupt the background sediment. Event layers 1-4 are characterized by grain-size that is coarser than the laminated background sediments, fining upwards trends from a sharp basal contact, and thicken towards the center of the lake basins. These characteristics and the absence of distinguishable event layers associated with historical flooding suggest that the four Ozette Lake event layers are seismically triggered turbidites. The units of alternating light and dark background laminae are too thick to be seasonal varves but have dominant periodicities of approximately 15 to 75 years which suggest they record the watershed and lake response to forcings, at least in part, by the Pacific Decadal

Oscillation. A comparison of three PDO indices to an event-free CT reveals a negative correlation between PDO phases and sediment density. The anticorrelation between PDO phases and sediment density is interpreted to result from increased regional precipitation and deposition of clastic sediment during negative phases of the PDO versus the less dense, more organic rich sediment during positive phases. This relationship between PDO phase and sediment color and density provides an independent (non-radiocarbon based) method to date event layers. Through the characterization of event layer sediments, radiocarbon dating, and application of two PDO-based dating techniques, the four Ozette Lake event layers likely record turbidites resulting from Cascadia Subduction Zone earthquakes Y, T2, W, and U. Ozette Lake sediments preserve both a record of late Holocene seismicity and variation in response to climate which can inform emergency response models for future CSZ ruptures.

References

1. Arhonditsis, G.B., Winder, M., Brett, M.T. and Schindler, D.E. (2004). Patterns and mechanisms of phytoplankton variability in Lake Washington (USA). Water Research, 38(18), pp.4013-4027.
2. Atwater, B. F., Carson, B., Griggs, G. B., Johnson, H. P., & Salmi, M. S. (2014). Rethinking turbidite paleoseismology along the Cascadia subduction zone. Geology, 42(9), pp. 827-830.
3. Atwater, B. F., Musumi-Rokkaku, S., Satake, K., Tsuji, Y., Ueda, K., & Yamaguchi, D. K. (2016). The orphan tsunami of 1700: Japanese clues to a parent earthquake in North America. University of Washington Press.
4. Atwater, B. F., Tuttle, M. P., Schweig, E. S., Rubin, C. M., Yamaguchi, D. K., & Hemphill-Haley, E. (2003). Earthquake recurrence inferred from paleoseismology. Developments in Quaternary Sciences, 1, pp. 331-350.
5. Atwater, B.F. (1987). Evidence for great Holocene earthquakes along the outer coast of Washington State. Science, 236(4804), pp. 942-944.
6. Atwater, B.F., Hemphill-Haley, E. (1997). Recurrence intervals for great earthquakes of the past 3,500 years at northeastern Willapa Bay, Washington. U.S. Geological Survey Professional Paper 1576, pp. 81-103.
7. Atwater, B.F., Musumi-Rokkaku, S., Satake, K., Tsuji, Y., Ueda, K., and Yamaguchi, D.K. (2005). The orphan tsunami of 1700—Japanese clues to a parent earthquake in North America (No. 1707).
8. Atwater, B.F., Nelson, A.R., Clague, J.J., Carver, G.A., Yamaguchi, D.K., Bobrowsky, P.T., Bourgeois, J., Darienzo, M.E., Grant, W.C., Hemphill-Haley, E. and Kelsey, H.M.

(1995). Summary of coastal geologic evidence for past great earthquakes at the Cascadia subduction zone. Earthquake spectra, 11(1), pp. 1-18.

9. Beaufort, L. and Grelaud, M. (2017). A 2700-year record of ENSO and PDO variability from the Californian margin based on coccolithophore assemblages and calcification. Progress in Earth and Planetary Science, 4(1), pp. 1-13.
10. Biondi, F., Gershunov, A., & Cayan, D. R. (2001). North Pacific decadal climate variability since 1661. Journal of climate, 14(1), pp. 5-10.
11. Blaauw, M. and Christen, J.A. (2011). Flexible paleoclimate age-depth models using an autoregressive gamma process. Bayesian analysis, 6(3), pp. 457-474.
12. Brandon, M. T., & Vance, J. A. (1992). Tectonic evolution of the Cenozoic Olympic subduction complex, Washington State, as deduced from fission track ages for detrital zircons. American Journal of Science, 292, pp. 565-565.
13. Cerda, M., Evangelista, H., Valdes, J., Siffedine, A., Boucher, H., Nogueira, J., Nepomuceno, A. and Ortlieb, L. (2019). A new 20th century lake sedimentary record from the Atacama Desert/Chile reveals persistent PDO (Pacific Decadal Oscillation) impact. Journal of South American Earth Sciences, 95:102302.
14. Clague, J. J., Bobrowsky, P. T., & Hutchinson, I. (2000). A review of geological records of large tsunamis at Vancouver Island, British Columbia, and implications for hazard. Quaternary Science Reviews, 19(9), pp. 849-863.
15. D'Arrigo, R. and Wilson, R. (2006). On the Asian expression of the PDO. International Journal of Climatology: A Journal of the Royal Meteorological Society, 26(12), pp.1607-1617.

16. D'Arrigo, R., Villalba, R., & Wiles, G. (2001). Tree-ring estimates of Pacific decadal climate variability. Climate Dynamics, 18(3-4), pp. 219-224.
17. DeMets, C., & Dixon, T. H. (1999). New kinematic models for Pacific-North America motion from 3 Ma to present, I: Evidence for steady motion and biases in the NUVEL-1A model. Geophysical Research Letters, 26(13), pp. 1921-1924.
18. Dong, B. and Dai, A. (2015). The influence of the interdecadal Pacific oscillation on temperature and precipitation over the globe. Climate Dynamics, 45(9-10), pp. 2667-2681.
19. Douglass, A. E. (1941). Crossdating in dendrochronology. Journal of Forestry, 39(10), pp. 825-831.
20. Fang, K., Chen, D., Ilvonen, L., Pasanen, L., Holmström, L., Seppä, H., Huang, G., Ou, T. and Linderholm, H. (2019). Oceanic and atmospheric modes in the Pacific and Atlantic Oceans since the Little Ice Age (LIA): Towards a synthesis. Quaternary Science Reviews, 215, pp. 293-307.
21. Garrison-Laney, C. (2017). Tsunamis and sea levels of the past millennium in Puget Sound, Washington. University of Washington (Doctoral dissertation).
22. Gedalof, Z. E., & Smith, D. J. (2001). Interdecadal climate variability and regime-scale shifts in Pacific North America. Geophysical Research Letters, 28(8), pp. 1515-1518.
23. Geiger, J., Hunyadfalvi, Z. and Bogner, P. (2009). Analysis of small-scale heterogeneity in clastic rocks by using computerized X-ray tomography (CT). Engineering Geology, 103(3-4), pp. 112-118.

24. Gilli, A., Anselmetti, F.S., Glur, L. and Wirth, S.B. (2013). Lake sediments as archives of recurrence rates and intensities of past flood events. In Dating torrential processes on fans and cones, pp. 225-242. Springer, Dordrecht.

25. Goff, J., Bobrowsky, P., Huntley, D., Sawai, Y., & Tanagawa, K. (2020). Palaeotsunamis along Canada's Pacific coast. Quaternary Science Reviews, 237:106309.

26. Goldfinger, C., C. H., Johnson, J. E., & Shipboard Scientific Party. (2003). Holocene earthquake records from the Cascadia subduction zone and northern San Andreas fault based on precise dating of offshore turbidites. Annual Review of Earth and Planetary Sciences, 31(1), pp. 555-577.

27. Goldfinger, C., Morey, A.E., Nelson, C.H., Gutiérrez-Pastor, J., Johnson, J.E., Karabanov, E., Chaytor, J., Eriksson, A. and Party, S.S. (2007). Rupture lengths and temporal history of significant earthquakes on the offshore and north coast segments of the Northern San Andreas Fault based on turbidite stratigraphy. Earth and Planetary Science Letters, 254(1-2), pp. 9-27.

28. Goldfinger, C., Nelson, C. H., & Johnson, J. E. (2003). Holocene Earthquake Records From the Cascadia Subduction Zone and Northern San Andreas Fault based on Precise Dating of Offshore Turbidites. Annual Review of Earth and Planetary Sciences, 31, pp. 555–577.

29. Goldfinger, C., Nelson, C.H., Morey, A.E., Johnson, J.E., Patton, J.R., Karabanov, E., Gutiérrez- Pastor, J., Eriksson, A.T., Gràcia, E., Dunhill, G., Enkin, R.J., Dallimore, A., Vallier, T. (2012). Turbidite Event History - Methods and Implications for Holocene Paleoseismicity of the Cascadia Subduction Zone. U.S. Geological Survey Professional Paper 1661–F pp. 332.

30. Håkanson, L. and Jansson, M. (1983). Principles of lake sedimentology (Vol. 316). Berlin: Springer-verlag.
31. Hamm, C.E. (2002). Interactive aggregation and sedimentation of diatoms and clay-sized lithogenic material. Limnology and Oceanography, 47(6), pp. 1790-1795.
32. Hare, S.R., Mantua, N.J., and Francis, R.C. (1999). Inverse production regimes: Alaska and west coast Pacific salmon. Fisheries, 24(1), pp. 6-14.
33. Hessl, A. E., McKenzie, D., & Schellhaas, R. (2004). Drought and Pacific Decadal Oscillation linked to fire occurrence in the inland Pacific Northwest. Ecological applications, 14(2), pp. 425-442.
34. Hormes, A., Blaauw, M., Dahl, S. O., Nesje, A., & Possnert, G. (2009). Radiocarbon wiggle-match dating of proglacial lake sediments–Implications for the 8.2 ka event. Quaternary Geochronology, 4(4), pp. 267-277.
35. Hutchinson, I., & Clague, J. (2017). Were they all giants? Perspectives on late Holocene plate-boundary earthquakes at the northern end of the Cascadia subduction zone. Quaternary Science Reviews, 169, pp. 29–49.
36. Kaplan, A., Kushnir, Y., & Cane, M. A. (2000). Reduced space optimal interpolation of historical marine sea level pressure: 1854–1992. Journal of Climate, 13(16), pp. 2987-3002.
37. Kastens, K.A. (1984). Earthquakes as a triggering mechanism for debris flows and turbidites on the Calabrian Ridge. Marine Geology, 55(1-2), pp. 13-33.
38. Kaufman, C.A., Lamoureux, S.F. and Kaufman, D.S. (2011). Long-term river discharge and multidecadal climate variability inferred from varved sediments, southwest Alaska. Quaternary Research, 76(1), pp. 1-9.

39. Keefer, D. K. (2002) Investigating landslides caused by earthquakes - A historical review. Surveys in Geophysics, 23, pp. 473–510.
40. Kirby, M. E., Lund, S. P., Patterson, W. P., Anderson, M. A., Bird, B. W., Ivanovici, L., Monarrez, P., and Nielsen, S. (2010). A Holocene record of Pacific decadal oscillation (PDO)-related hydrologic variability in southern California (Lake Elsinore, CA). Journal of Paleolimnology, 44.3, pp. 819-839.
41. Leithold, E. L., Wegmann, K. W., & Bohnenstiehl, D. R. (2017, October). A Holocene earthquake record from Lake Crescent, Olympic Peninsula, Washington. In GSA Annual Meeting in Seattle, Washington, USA-2017. GSA.
42. Leithold, E. L., Wegmann, K. W., Bohnenstiehl, D. R., Joyner, C. N., & Pollen, A. F. (2019). Repeated megaturbidite deposition in Lake Crescent, Washington, USA, triggered by Holocene ruptures of the Lake Creek-Boundary Creek fault. GSA Bulletin.
43. MacDonald, G.M. and Case, R.A. (2005). Variations in the Pacific Decadal Oscillation over the past millennium. Geophysical Research Letters, 32(8).
44. Mantua, N. J., & Hare, S. (2002). Pacific-Decadal Oscillation (PDO). Encyclopedia of global environmental change, 1, pp. 592-594.
45. Mantua, N. J., Hare, S. R., Zhang, Y., Wallace, J. M., & Francis, R. C. (1997). A Pacific interdecadal climate oscillation with impacts on salmon production. Bulletin of the American Meteorological Society, 78(6), pp. 1069-1080.
46. McCaffrey, R., Qamar, A. I., King, R.W., Wells, R., Khazaradze, G., Williams, C.A., Stevens, C.W., Vollick, J.J., and Zwick, P.C. (2007). Fault locking, block rotation and crustal deformation in Pacific Northwest. Geophysical Journal, 169, pp. 1315-1340.

47. McMillan, A. D., & Hutchinson, I. (2002). When the mountain dwarfs danced: Aboriginal traditions of Paleoseismic events along the Cascadia subduction zone of Western North America. Ethnohistory, 49(1), pp. 41-68.

48. McMillan, A.D. (1999). Since the Time of the Transformers: The Ancient Heritage of the Nuu-Chah-Nulth, Ditidaht and Makah, UBC Press.

49. Moernaut, J., De Batist, M., Heirman, K., Van Daele, M., Pino, M., Brümmer, R. and Urrutia, R. (2009). Fluidization of buried mass-wasting deposits in lake sediments and its relevance for paleoseismology: results from a reflection seismic study of lakes Villarrica and Calafquén (South-Central Chile). Sedimentary Geology, 213(3-4), pp. 121-135.

50. Moernaut, J., Van Daele, M., Heirman, K., Fontijn, K., Strasser, M., Pino, M., Urrutia, R., and De Batist, M. (2014). Lacustrine turbidites as a tool for quantitative earthquake reconstruction: New evidence for a variable rupture mode in south central Chile. Journal of Geophysical Research: Solid Earth, 119. 3, pp. 1607-1633.

51. Moernaut, J., Van Daele, M., Strasser, M., Clare, M.A., Heirman, K., Viel, M., Cardenas, J., Kilian, R., de Guevara, B.L., Pino, M. and Urrutia, R. (2017) Lacustrine turbidites produced by surficial slope sediment remobilization: a mechanism for continuous and sensitive turbidite paleoseismic records. Marine Geology, 384, pp. 159-176.

52. Monecke, K., Anselmetti, F.S., Becker, A., Sturm, M. and Giardini, D. (2004). The record of historic earthquakes in lake sediments of Central Switzerland. Tectonophysics, 394(1-2), pp. 21-40.

53. Nelson, A. R., Kelsey, H. M., & Witter, R. C. (2006). Great earthquakes of variable magnitude at the Cascadia subduction zone. Quaternary Research, 65(3), pp. 354-365.

54. Newman, M., Alexander, M.A., Ault, T.R., Cobb, K.M., Deser, C., Di Lorenzo, E., Mantua, N.J., Miller, A.J., Minobe, S., Nakamura, H. and Schneider, N. (2016). The Pacific decadal oscillation, revisited. Journal of Climate, 29(12), pp. 4399-4427.

55. National Oceanic and Atmospheric Administration (1999). Endangered and threatened species—Threatened status for Ozette Lake sockeye salmon in Washington: Federal Register, v. 64, no. 57, pp. 14528–14536.

56. Reilly, B.T., Stoner, J.S. and Wiest, J. (2017). Sed CT: MATLAB™ tools for standardized and quantitative processing of sediment core computed tomography (CT) data collected using a medical CT scanner. Geochemistry, Geophysics, Geosystems, 18(8), pp. 3231-3240.

57. Reimer, P.J., Bard, E., Bayliss, A., Beck, J.W., Blackwell, P.G., Ramsey, C.B., Buck, C.E., Cheng, H., Edwards, R.L., Friedrich, M. and Grootes, P.M. (2013). IntCal13 and Marine13 radiocarbon age calibration curves 0–50,000 years cal BP. Radiocarbon, 55(4), pp. 1869-1887.

58. Rey, F., Gobet, E., Szidat, S., Lotter, A. F., Gilli, A., Hafner, A., & Tinner, W. (2019). Radiocarbon wiggle matching on laminated sediments delivers high-precision chronologies. Radiocarbon, 61(1), pp. 265-285.

59. Ritchie, A., & Bourgeois, J. (2009). Late Quaternary Sediment Source and Deposition History of Ozette Lake. U.S. Department of the Interior, National Park Service, Technical Report.

60. Satake, K., K. Shimazaki, Y. Tsuji, and K. Uyeda. (1996). Time and Size of a Great Earthquake in Cascadia Inferred from Japanese Tsunami Records of January 1700. Nature, 379, pp. 246–249.

61. Schasse, H.W. (2003). Geologic map of the Washington portion of the Port Angeles 1:100,000 quadrangle. Washington Division of Geology and Earth Resources Open File Report, 1 Sheet.

62. Schneider, N., & Cornuelle, B. D. (2005). The forcing of the Pacific decadal oscillation. Journal of Climate, 18(21), pp. 4355-4373.

63. Snavely, P. D., Jr.; MacLeod, N. S.; Niem, A. R.; et al. (1993). Geologic map of the Cape Flattery, Clallam Bay, Ozette Lake, and Lake Pleasant quadrangles, northwestern Olympic Peninsula, Washington: U.S. Geological Survey Miscellaneous Investigations Series Map I-1946, 1 sheet, scale 1:48,000.

64. Snowball, I., Muscheler, R., Zillen, L., Sandgren, P., Stanton, T., & Ljung, K. (2010). Radiocarbon wiggle matching of Swedish lake varves reveals asynchronous climate changes around the 8.2 kyr cold event. Boreas, 39(4), pp. 720-733.

65. Steinman, B.A., Abbott, M.B., Mann, M.E., Stansell, N.D. and Finney, B.P. (2012). 1,500 year quantitative reconstruction of winter precipitation in the Pacific Northwest. Proceedings of the National Academy of Sciences, 109(29), pp. 11619-11623.

66. Strasser, M., Monecke, K., Schnellmann, M. and Anselmetti, F.S. (2013). Lake sediments as natural seismographs: A compiled record of Late Quaternary earthquakes in Central Switzerland and its implication for Alpine deformation. Sedimentology, 60(1), pp. 319-341.

67. Sun, Q., Xie, M., Shi, L., Zhang, Z., Lin, Y., Shang, W., Wang, K., Li, W., Liu, J. and Chu, G. (2013). Alkanes, compound-specific carbon isotope measures and climate

variation during the last millennium from varved sediments of Lake Xiaolongwan, northeast China. Journal of paleolimnology, 50(3), pp. 331-344.

68. Thrush, C., & Ludwin, R. S. (2007). Finding fault: Indigenous seismology, colonial science, and the rediscovery of earthquakes and tsunamis in Cascadia. American Indian Culture and Research Journal, 31(4), pp. 1-24.
69. Urban, F. E., Cole, J. E., & Overpeck, J. T. (2000). Influence of mean climate change on climate variability from a 155-year tropical Pacific coral record. Nature, 407(6807), pp. 989-993.
70. Van Daele, M., Araya-Cornejo, C., Pille, T., Vanneste, K., Moernaut, J., Schmidt, S., Kempf, P., Meyer, I. and Cisternas, M. (2019). Distinguishing intraplate from megathrust earthquakes using lacustrine turbidites. Geology, 47(2), pp. 127-130.
71. Van Daele, M., Moernaut, J., Doom, L., Boes, E., Fontijn, K., Heirman, K., Vandoorne, W., Hebbeln, D., Pino, M., Urrutia, R. and Brümmer, R. (2015). A comparison of the sedimentary records of the 1960 and 2010 great Chilean earthquakes in 17 lakes: Implications for quantitative lacustrine palaeoseismology. Sedimentology, 62(5), pp. 1466-1496.
72. Vandekerkhove, E., Van Daele, M., Praet, N., Cnudde, V., Haeussler, P.J. and De Batist, M. (2020). Flood-triggered versus earthquake-triggered turbidites: A sedimentological study in clastic lake sediments (Eklutna Lake, Alaska). Sedimentology, 67(1), pp. 364-389.
73. Vo, A. M. (2019). Multi-proxy approach to reconstructing a paleoseismic record of cascadia subduction zone earthquakes in late holocene sediments of lake crescent, WA. Raleigh, North Carolina: North Carolina State University.

74. Wells, R.E., Weaver, C.S., Blakely, R.J. (1998). Fore-arc migration in Cascadia and its neotectonic significance. Geology, 26(8), pp. 759-762.

75. Woodward, A., Haggerty, M., and Crain, P. (2019). Life-history model for sockeye salmon (*Oncorhynchus nerka*) at Lake Ozette, northwestern Washington—Users' guide: U.S. Geological Survey Open File Report 2019-1031.

76. Wray, J., & Anderson, M. K. (2003). Restoring Indian-set fires to prairie ecosystems on the Olympic Peninsula. Ecological Restoration, 21(4), pp. 296-301.

77. Zhang, Y., Wallace, J. M., & Battisti, D. S. (1997). ENSO-like interdecadal variability: 1900–93. Journal of climate, 10(5), pp. 1004-1020.

78. Zolitschka, B. (1996). High resolution lacustrine sediments and their potential for palaeoclimatic reconstruction. In Climatic variations and forcing mechanisms of the last 2000 years (pp. 453-478). Springer, Berlin, Heidelberg.

79. Zolitschka, B., Francus, P., Ojala, A.E. and Schimmelmann, A. (2015). Varves in lake sediments–a review. Quaternary Science Reviews, 117, pp.1-41.